JOINT EUROPEAN TORUS

JET–P(91)09

P. C. Stangeby, J.D. Elder
and JET Team

Some Possibilities for Measuring Local Plasma Parameters in the Edge Plasma By Impurity Injection

"This document contains JET information in a form not yet suitable for publication. The report has been prepared primarily for discussion and information within the JET Project and the Associations. It must not be quoted in publications or in Abstract Journals. External distribution requires approval from the Publications Officer, JET Joint Undertaking, Abingdon, Oxon, OX14 3EA, UK".

"Enquiries about Copyright and reproduction should be addressed to the Publications Officer, EFDA, Culham Science Centre, Abingdon, Oxon, OX14 3DB, UK."

The contents of this preprint and all other JET EFDA Preprints and Conference Papers are available to view online free at www.iop.org/Jet. This site has full search facilities and e-mail alert options. The diagrams contained within the PDFs on this site are hyperlinked from the year 1996 onwards.

Some Possibilities for Measuring Local Plasma Parameters in the Edge Plasma By Impurity Injection

P. C. Stangeby, J.D. Elder
and JET Team*

JET-Joint Undertaking, Culham Science Centre, OX14 3DB, Abingdon, UK

University of Toronto Institute for Aerospace Studies, Downsview, Ontario, Canada
** See Appendix 1*

Preprint of Paper to be submitted for publication in
Plasma Physics and Controlled Fusion

Draft: April 5, 1991

SOME POSSIBILITIES FOR MEASURING LOCAL PLASMA PARAMETERS IN THE EDGE PLASMA BY IMPURITY INJECTION

P. C. Stangeby and J. D. Elder

University of Toronto Institute for Aerospace Studies
4925 Dufferin Street
Downsview, Ontario, Canada
M3H 5T6

and

JET Joint Undertaking
Abingdon, Oxon, U.K.
OX14 3EA

Abstract

Some opportunities for measuring n_e, T_e, T_i, Z_{eff} and background plasma drift velocities in the edge region of magnetic confinement devices based on impurity injection are described. The technique would be based on spatially resolving (along $\vec{B}$) the distributions of successive charge states and the measurement of (Doppler) temperatures of the states. Some simple analytic relations can be obtained to permit the extraction of first order estimates of the plasma parameters, one at a time, from the experimental data; however, in practice, it will generally be necessary to use an impurity transport code with the input plasma parameters varied to obtain a best fit to all of the available experimental data simultaneously.

Introduction

In order to improve our understanding of the plasma edge, localized measurements are needed of electron temperature T_e, deuterium ion temperature T_{D+}, electron density n_e, effective charge state Z_{eff}, and deuterium ion drift velocity v_{D+}. In principle, it should be possible to measure these quantities using localized spectroscopic measurements of the spatial distribution along $\vec{B}$ of successive charge states of injected impurities and the measured average (Doppler) temperatures of the different charge states. Such spatially resolved measurements have been made recently on TEXTOR using a CO puff [1,2], although no attempt was made there to employ the method as a diagnostic tool. Impurity injection has also been successfully employed on TEXTOR using Li beams and laser blow-off to measure edge temperatures and densities from the radial attenuation of the impurity fluxes [3, 4].

The experimental arrangement proposed here would ideally consist of a short time pulse injection in the cross-field direction of a narrow beam of impurities. Spectroscopic viewing would be at right angles to the axis of the beam, Fig. 1, and ideally should provide spatial resolution both along $\vec{B}$, and along the beam axis. This arrangement differs from that employed in TEXTOR [3, 4] where the impurity source is viewed only in the radial direction. Such an injection might be achieved, for example, by firing a pellet into the plasma. The pellet mass and velocity would have to be adjusted to produce a sufficient signal, but not to change the edge plasma conditions. Other arrangements are possible and injection methods which are less than ideal could still yield diagnostic information, although the data interpretation would be more complicated. Two-dimensional viewing would most readily be provided by using CCD cameras fitted with appropriate light filters [1]; time resolution, if needed, would require fast gating and an image intensifier. One-dimensional viewing (along $\vec{B}$) would provide information at a single radius. The arrangement shown in Fig. 1 requires two

ports on the tokamak vessel. A single port arrangement has been employed in the MIT Li pellet (q-profile) experiment on TFTR with viewing co-linear to the pellet trajectory [5]; the distribution of impurities along $\vec{B}$ at different radial depths into the plasma is achieved by time resolution.

The spatial distributions of the density and temperature of successive impurity charge states are dependent on the plasma parameters n_e, T_e, T_{D+}, Zeff and v_{D+}, usually nonlinearly. Generally, so much information is contained in these spatial distributions that it should be possible to interpret the observations with an impurity transport code such as LIM [6-8] so as to extract all these plasma parameters, with sufficient additional information available to provide consistency checks. Interpretation would be simplest if the states being observed were so short-lived that cross-field transport could be ignored. For typical divertor plasma conditions this would generally limit the charge states to $q < 3$. In order to demonstrate the diagnostic possibilities, only such simple examples will be described in this report; furthermore, examples will describe situations where each plasma parameter could be separately extracted, one at a time. In fact, use of an impurity transport code such as LIM, which includes cross-field transport, would make it useful to follow all the charge states which can be observed. Extraction of the plasma parameters could then generally not be achieved one at a time, but would require an optimization procedure to find the plasma parameters — now including the diffusion coefficient $D_\perp(r)$ — which would give the best match of code and experimental results.

Reiterating, the analysis can be carried out sequentially, one parameter at a time, in order to obtain initial approximations to the values of the plasma parameters, possibly from analytic expressions; a proper analysis, however, will require the use of an impurity transport code such as LIM with the input plasma parameters varied so as to obtain a best fit to all of the experimental data simultaneously. This paper focuses on the former procedure.

Measuring n_e and T_e

The electron density and temperature are the most basic plasma parameters in the edge. They are important to know in their own right, and also because they are needed in the evaluation of the other plasma parameters, T_{D^+}, Z_{eff}, V_{D^+}. These two quantities are presently measured by various methods including Langmuir probes by the impurity injection techniques developed on TEXTOR [3, 4], etc. The impurity injection arrangement proposed here would provide further opportunities to measure n_e and T_e.

The spatial extent along $\vec{B}$ of the impurity neutrals is largely dependent on n_e and T_e only — a situation which also often characterizes the lowest charge ion states, although a weak dependence on the other plasma parameters can arise. A further simplification occurs over specific ranges of T_e for specific impurity species: the spatial extents are insensitive to T_e when the neutral ionization rate coefficient $\overline{\sigma v}_{iz}$ is approximately constant. In Fig. 2 are shown ionization mean free paths, λ_{iz}, for various elements and charge states assuming impurity particle energy of 15 eV, characteristic of physical sputtering, and $n_e = 10^{19}$ m^{-3}. For Li^o, for example, λ_{iz} varies by ±10% at most for $12 \lesssim T_e \lesssim 150$ eV. Thus, from a measurement of the absolute value of λ_{iz}, n_e can be directly deduced.

As is also evident from Fig. 2, the λ_{iz} values of some other species are strongly dependent on T_e in certain ranges of T_e. Thus, from a measurement of the ratio of λ_{iz} for two different species — one with a strong dependence on T_e, the other with a weak one — T_e can be deduced independently of n_e. Figure 3 shows some examples of potentially useful λ_{iz} ratios. Generally it is possible, for each temperature range, to find a pair of states which give a change in the λ-ratio of 2 for a change in T_e of a factor of about 2. The highest sensitivities, however, generally require the injection of

more than one element. Thus, the use of composite pellets is indicated, or the successive use of pellets of different elements.

The LIM impurity code [6-8] was used to predict the time-integrated spatial profiles resulting from a 4 mm diameter pellet crossing $\vec{B}$ at right angles. For simplicity in this illustration of principle it was assumed that neutrals were launched uniformly over a zone spanning ±2 mm from the centre of the trajectory, with a single energy of 15 eV and with equal probability in the ± direction along $\vec{B}$, i.e., a 1-D launch. In reality, physical sputtering results in a Thompson velocity distribution [9], and a particular angular distribution [10]; LIM examples for such distributions are also shown below. Particles subject to thermal evaporation will be discussed later. An example of the spatial distributions assuming 15 eV carbon atoms is given in Fig. 4. For such a launch assumption it is readily shown that the spatial distribution of the neutrals and for the q = 1 ions are:

Neutrals:

$$P^o(y) = \begin{cases} \frac{\tau_o}{4\Delta}\left(2-\exp[(y-\Delta)/\lambda_o] - \exp[-(y+\Delta)/\lambda_o]\right), & y < \Delta \\ \frac{\tau_o}{4\Delta}\left[\exp -y/\lambda_o\right]\left[\exp(\Delta/\lambda_o) - \exp(-\Delta/\lambda_o)\right], & y > \Delta \end{cases} \qquad (1)$$

1st Ionization Stage:

$$P^1(y) = \left(\text{for } y < \Delta\right) \begin{cases} \frac{\tau_1}{4\Delta}\Big[2-\exp[-(y+\Delta)/\lambda_1] - \exp[(y-\Delta)/\lambda_1] \\ \quad - (\lambda_1/\lambda_o - 1)^{-1}\left(\exp[-y/\lambda_1 - \Delta/\lambda_o]\right. \\ \quad\quad \left[\exp(\Delta/\lambda_{01}) - \exp(-y/\lambda_{01})\right] \\ \quad - (\lambda_1/\lambda_o)^{-1}\left(\exp[y/\lambda_1 - \Delta/\lambda_o]\right) \\ \quad\quad \left.\left[\exp(\Delta/\lambda_{o1} - \exp(y/\lambda_{o1})\right]\right] \end{cases} \qquad (2a)$$

$$P^1(y) = \left(\text{for } y > \Delta\right) \begin{cases} \frac{\tau_1}{4\Delta}\Big[\exp(-y/\lambda_1)\,[\exp(\Delta/\lambda_1) - \exp(-\Delta/\lambda_1) \\ \quad - (\lambda_1/\lambda_o - 1)^{-1}\left(\exp(-\Delta/\lambda_o)\right)[\exp(\Delta/\lambda_{o1}) - \exp(-\Delta/\lambda_{o1})] \\ + (\lambda_1/\lambda_o - 1)^{-1}\left(\exp(\Delta/\lambda_o) - \exp(-\Delta/\lambda_o)\right)[\exp(-\Delta/\lambda_{o1}) - \exp(-y/\lambda_{o1})]\Big]\Big] \end{cases} \quad (2b)$$

where τ_o, τ_1 are the average ionization times (from original launch) for neutrals and q = 1 ions, e.g., $\tau_o = (n_e\,\overline{\sigma v}^{o}_{iz})^{-1}$; the source is uniformly distributed along $\vec{B}$ (the y-direction) over $\pm\Delta$; λ_o, λ_1 are the ionization mean-free-paths, e.g., $\lambda_o = v_o\tau_o$ where v_o is the neutral launch velocity along y; $1/\lambda_{o1} \equiv 1/\lambda_o - 1/\lambda_1$.

One should note that the spatial distribution of q = 1 ions, $P^1(y)$, given here neglects all collisional processes with the background plasma ions. In the LIM code, however, the stopping, heating-up and parallel-diffusion collisions are included, and so one would anticipate some discrepancy between $P^1(y)$, Eq. (2), and the LIM-calculated profiles. From the example shown in Fig. 4, the agreement for both C^o and C^+ with Eqs. (1), (2) is seen, in fact, to be quite good. The reason for the good C^+ agreement is that for the case shown the C^+ ions are not very collisional; this case assumed $n_e = 10^{19}$ m^{-3}, $T_e = T_{D+} = 100$ eV, $Z_{eff} = 1$ which gives for the various characteristic times: $\tau_1 = 3.6$ μs, τ_S (Spitzer stopping time) = 710 μs, τ_T (Spitzer thermalization time) = 400 μs, $\tau_{||}$ (Spitzer diffusion time) = 125 μs.

As is evident from Eqs. (1), (2), the profiles behave exponentially for large y, with characteristic decay lengths of λ_o and λ_1, as expected. Similar results hold for higher ionization stages, under the same assumption of neglecting ion collisions. For the current example, the profiles for stages up to C^{3+} are shown in Fig. 5 and as can be seen, the exponential behaviour is still approximately followed up to C^{3+} with decay lengths not too far from the simply-calculated ones (which assumes particles simply continue to move along $\vec{B}$ with velocity v_o as they proceed to higher stages of ionization). For C^{3+} one has $\tau_3 = 97$ μs, $\tau_S = 79$ μs, $\tau_T = 45$ μs, $\tau_{||} = 67$ μs ($\bar{T}^{C+} = 73$

eV) and so collisionality is marginal. For such cases, it is then reliable to extract values of T_e from the ratio of λ_{iz}'s for the lowest ionization stages, Fig. 3. From Fig. 5 one finds $\lambda_0 = 0.014$ m, $\lambda_1 = 0.060$ m, $\lambda_2 = 0.28$ m, $\lambda_3 = 1.73$ m which may be compared with the values simply calculated, i.e., $v_0\tau_0$, etc., which are: $\lambda_0 = 0.014$ m, $\lambda_1 = 0.056$ m, $\lambda_2 = 0.28$ m, $\lambda_3 = 1.49$ m.

By contrast, a LIM case assuming $T_e = T_{D+} = 25$ eV, $n_e = 10^{19}$ m^{-3}, $Z_{eff} = 1$ produces profiles which are fairly close approximations to exponential shapes in the wings but the exponential scale lengths, $\lambda_0/\lambda_1/\lambda_2/\lambda_3 = 0.028/0.15/0.92/1.74$ m were in disagreement with the simply-calculated values for C^{2+} and C^{3+}: $\lambda_0/\lambda_1/\lambda_2/\lambda_3 = 0.027/0.18/1.4/13$. The C^0 and C^+ profiles were still as simply calculated which was expected from the collision times, since the C^+ was only slightly collisional while the C^{2+} and C^{3+} were strongly collisional.

Table 1 gives the LIM-values of λ_0, etc., for various cases assuming 15 eV lithium or carbon neutrals, with comparisons to the simply-calculated values. As can be seen, for the range of conditions examined the Li^0 and C^+ profiles are not very sensitive to changes in T_{D+} or Z_{eff}, and are primarily functions of T_e and n_e (with Li^0 being approximately dependent on n_e only). The ratio of $\lambda_{C+}/\lambda_{Li0}$ is therefore a good indicator of T_e; as shown in Table 1, the average error in the inferred values of T_e was only 8% for this set of cases. The absolute value of λ_{Li0} provides a good measure of n_e; results are also given in Table 1 where the n_e values were calculated from the LIM-values of λ_{Li0} assuming 15 eV neutrals and $\overline{\sigma v}_{iz} = 8.5\text{x}10^{-14}$ m^{-3} sec^{-1} for all cases. The other values of λ are generally less reliably given by the slopes of the LIM-calculated profiles, and the use of these higher states to extract n_e and T_e should be done using an impurity transport code. Nevertheless, these values of λ can provide an approximate measure of T_e; as shown in Table 1 the average errors using $\lambda_{C2+}/\lambda_{Li0}$, $\lambda_{Li+}/\lambda_{Li0}$, $\lambda_{C+}/\lambda_{C0}$, $\lambda_{C2+}/\lambda_{C0}$, $\lambda_{C2+}/\lambda_{C+}$, $\lambda_{Li+}/\lambda_{C+}$ were 14%, 18%, 19%, 29%, 37%, 54% respectively, for this set of cases.

The method proposed here for measuring n_e and T_e from λ_{iz} values is the parallel-to-$\vec{B}$ equivalent to the cross-$\vec{B}$ method developed on TEXTOR [3,4], with the added aspect that the profiles of the ionized states provide additional useful data.

More realistic assumptions may be made about the velocity and angular distributions of the neutrals at their point of release. Some such elaborations can still be followed analytically, although the most realistic modelling can only be done with a code. An extension which can still be approximately reproduced analytically assumes the Thompson velocity distribution, including a maximum velocity cut-off and an isotropic angular distribution. One can also allow for the source to be spatially distributed, although this makes for particularly complicated analytic expressions. Here it is assumed that all the neutrals are launched at a single value of y. The neutral distribution can be shown to be:

$$P^o(x) = \left[\xi_{max}(2E_{bd}/m_I)^{1/2}(2/\pi)\right]^{-1}\left[\exp(-xp)\left((2p+1)(p+1)^{-2} + x(p+1)^{-1}\right)\right.$$
$$\left. - x\exp(x)\,E_1(x(p+1))\,(2+x)\right] \qquad (3)$$

where

x	$\equiv$	fy/λ_o
λ_o	$=$	$f(2/\pi)(2E_{bd}/m_I)^{1/2}\tau_o$
E_{bd}	$=$	surface binding energy (8.3 eV for C, 1.7 eV for Li)
m_I	$=$	mass of impurity particle
ξ_{max}	$=$	$(1 + E_{bd}/E_{max})^{-2}$
E_{max}	$=$	maximum energy of sputtered neutral
	$=$	$E_{impact}\,\gamma(\gamma-1) - E_{bd}$
E_{impact}	$=$	energy of ion impacting on the pellet
γ	$=$	$4m_{impact}\,m_I\,(m_{impact} + m_I)^{-2}$

$$f = \xi_{max}^{-1} \int_0^{\xi_{max}} (\xi^{-1/2} - 1)^{-1/2} d\xi$$

$$p = \xi_{max}^{-1/2} - 1$$

$$E_1(z) \equiv \int_z^{\infty} e^{-t} t^{-1}\, dt, \text{ the exponential integral}$$

and the factor $(2/\pi)$ gives the average projection of the velocity vector along $\vec{B}$ for isotropic launch. This distribution only applies to the neutrals, but also gives a first approximation to the first few ionization states — again, assuming as before, that ion collisions can be neglected. Comparisons are made in Fig. 6 between this analytic result and LIM results for the states up to C^{3+} with the same plasma background assumed as before. The simply-calculated values of the λ's: $\lambda_0 = 10.7$ mm, $\lambda_1 = 50$ mm, $\lambda_2 = 139$ mm, $\lambda_3 = 890$ mm. For the ions, Eq. (3) does not give the peak correctly and so in Fig. 6 the analytic expression is matched to the LIM result at one location (at $y_j = \lambda_j/f$). Equation (3) also does not fit the neutral peak precisely, because of the approximate method of dealing with the angular distribution in the analytic expression, and so here also the match was made at $y = \lambda_0/f$. The same general conclusions follow as for the monovelocity case, namely, that the profiles (except near the peaks) can be used to extract λ_{iz} reliably for the neutrals, and to a good approximation for the first few ion stages — at least for plasmas as weakly collisional as the example here.

Measuring T_i and Z_{eff}

The degree of thermalization of the impurity ions is dependent on T_e, T_i, n_e and Z_{eff}. If n_e and T_e have been measured, as by the foregoing method or otherwise, the

values of T_i and Z_{eff} can then be inferred from spectroscopic (Doppler) temperature measurements of successive charge states. Such measurements need not be spatially resolved since a spatial average for the charge state provides sufficient information. Any information on the spatial distribution of the impurity temperatures, however, is very useful and provides consistency checks; examples of LIM-calculated spatial distributions of impurity ion temperature are shown below.

It can be shown that the average temperature of ion charge state q is given approximately by

$$\bar{T}_q \approx \bar{T}_{q-1} + (T_i - \bar{T}_{q-1})(1+\tau_{T_q}/\tau_q)^{-1} \qquad (4)$$

where τ_{T_q} is the Spitzer thermalization time of state q, τ_q is, as before, the average ionization time of state q, and T_i is the background, e.g., deuterium, ion temperature. One may note a useful feature from Eq. (4), namely, there is no dependence on n_e since it cancels out in the τ_{T_q}/τ_q ratio. The ratio $\tau_{T_q}/\tau_q \propto T_i^{3/2} q^{-2} Z_{eff}^{-1} \overline{\sigma v}_{izq}$ and thus from a measurement of the temperature of three successive charge states, together with a knowledge of T_e, i.e., $\overline{\sigma v}_{iz}$, one can deduce both T_i and Z_{eff}. Although it is not immediately obvious, it often turns out to be the case that uncertainty in the value of T_e has only a relatively small influence on the value of T_i deduced.

By way of illustration, the same case as discussed above gave the following LIM-calculated temperatures: $\bar{T}_{C+}$ = 15.8 eV, $\bar{T}_{C2+}$ = 26.4 eV, $\bar{T}_{C3+}$= 73.2 eV. If one assumes that T_e = 100 eV then the use of Eq. (4) together with these impurity temperatures gives T_{D+} = 99.5 eV, Z_{eff} = 1.01 which are very close to the values assumed as input for this case. The effect of uncertainty in the value of T_e primarily influences the deduced value of Z_{eff}; the assumption of T_e = 50 (200) eV in Eq. (4) gave for this case T_{D+} = 101 (130) eV, Z_{eff} = 0.55 (1.26). That is, an uncertainty of a

factor 2 in T_e gives an uncertainty in T_{D+} of ~15% and ~25% in Z_{eff} for this case. The fact that $Z_{eff} \geq 1$ is required places a limit on the effect of uncertainties.

A second LIM example using as input assumptions $T_e = T_{D+} = 50$ eV, $n_e = 10^{19}$ m^{-3} and $Z_{eff} = 3$ found $\bar{T}_{C+} = 18.6$ eV, $\bar{T}_{C2+} = 40.4$ eV, $\bar{T}_{C3+} = 49.7$ eV. Application of Eq. (4) assuming $T_e = 50$ eV gave $T_{D+} = 49.99$ eV, $Z_{eff} = 3.004$. Assuming $T_e =$ 30 (70) eV gave as output $T_{D+} = 49.97$ (50.1) eV, $Z_{eff} = 1.49$ (4.11); in this case a negligible uncertainty in T_{D+} but a larger, ~45%, uncertainty in Z_{eff}. The Z_{eff}-uncertainties are thus about the same or smaller than the T_e-uncertainty; of course, the effect of uncertainties in the measured $\bar{T}_{imp}$ also have to be included.

For cases where T_{D+} is near the value of the neutral impurity temperature associated with physical sputtering, it may be advantageous to employ pellets which will produce colder neutrals, so as to spread out the successive charge state temperatures over a reasonably large range (to deduce Z_{eff}). This could be achieved with ablative/evaporative pellets. An attractive possibility would be frozen CO pellets since CO is known to break up into ~0.05 eV atoms and ions [1,2,6]. An additional advantage to employing pellets with two elements is that the quantity of data essentially doubles, providing many consistency checks.

Spatial resolution of impurity temperatures would provide further data for deducing T_i and Z_{eff}. Figures 7a and 7b show examples of LIM-calculated temperature distributions for two different values of Z_{eff}. Fitting of the spatial shape and absolute magnitude of the temperature of even a single stage of the impurity may be adequate to deduce both T_i and Z_{eff}. The effect of starting at low neutral temperatures is incorporated here with the source assumption of 0.25 eV, isotropic (sublimation) carbon neutrals being used in these cases.

Measuring v_{D+}

The sink action of limiters and divertor target plates for impurity ions is largely dependent on the force of friction due to the deuterium drift velocity v_{D+}. Other forces also operate on impurity ions, including electric fields and temperature gradient forces, but in many situations these forces are less important than friction [12]. It is therefore important to establish the magnitude of v_{D+}, and also the drift direction since for a highly recycling divertor flow reversal may occur, a process which could transport divertor impurities toward the main plasma. Plasma flows at the edge have also been implicated in enhanced confinement regimes of tokamaks where plasma rotation is associated with radial electric fields and altered cross-field transport [13].

If the deuterium ions are drifting, then the spatial distribution of the impurities will be skewed. The degree of skewness will depend on v_{D+} — also on n_e, T_e, T_{D+}, Z_{eff} which would have to be measured as above or otherwise. An example of carbon profiles is given in Fig. 8 for $v_{D+} = 2 \times 10^4$ m/s to the left and purely along the $\vec{B}$ direction (no poloidal drifts). Other plasma conditions are given in the caption. Defining skewness as the ratio of, say, the C^{2+} density at ±5 cm either side of the injection point, one has a measure of v_{D+}, Fig. 9. Some examples of Fe^{2+} are also shown in Fig. 9. Figure 10 shows examples of C^0, C^+, C^{2+}, C^{3+} profiles for two different neutral energies, 0.05 eV (as from dissociating CO) and 15 eV (as from physical sputtering). Assumed background: $T_e = T_{D+} = 50$ eV, $n_e = 10^{19}$ m^{-3}, $Z_{eff} = 1$. Although the profiles are quite different for the two launch energies, the sensitivity to drift velocity does not differ substantially. The differences with the more collisional example of Fig. 8, however, is marked. The impurity collision rate varies as $q^2 Z_{eff} T_{D^+}^{-3/2}$ and thus the asymmetries are as dependent on this quantity as on v_{D+}.

The skewness patterns shown in Figs. 8 and 10 can be related to simple analytic derivations, at least as to their broad features. Provided the ion species is not too

collisional the extent of the profile upstream is given by the distance required to stop the ions by friction, based on the initial neutral velocity. The upstream profiles also clearly include particles which have travelled further upstream by diffusion. The extent of the profile downstream can be estimated by similar methods.

When other forces than friction are operative, then the skewness is no longer a measure of v_{D+} but of the net force on the impurities. Often, however, it is the net impurity force which is of primary interest in any event. In such cases, it would be preferable to employ injected impurity species which are close in mass and charge to the impurity species whose transport is of interest since the net force can have a complex dependence on m and q.

Signal Strength and Plasma Disturbance

The impurity injection must be sufficiently massive to provide a measurable signal, yet not perturb the edge plasma. On TEXTOR the Li thermal oven must produce ~$2x10^{14}$ Li/s in order to provide an adequate signal from the LiI resonance line at 6708Å for the Si-diode array camera and filter system [11]. That system integrates in time over 0.5 ms and spatially over the two directions perpendicular to the injection axis; the LiI is typically distributed over about 5 cm along the axis. Thus about 10^{10} Li are needed per cm of axial length per frame. For a 4 mm diameter pellet releasing neutrals by physical sputtering, thus $\lambda_o \approx 1$ cm, there will be of order 10^{22} Li/m^2/s injected into the flux tube (along $\vec{B}$) (assuming $n_e \approx 10^{19}$ m^{-3}, $T_e \approx T_{D+} \approx 50$ eV, and a sputtering yield of a few percent). For a pellet moving at 100 m/s, therefore, about 10^{14} Li atoms will be injected per cm of its trajectory, entering a flux tube of cross-sectional area about 1 cm^2. Since this is about 10^4 times larger than the level required to provide a measurable signal it should be adequate even when allowance is

made for the fact that non-resonance lines may be involved for other states of interest and that enough signal is required to measure spatial profiles along $\vec{B}$.

With regard to disturbing the edge plasma, this will be a problem for ablative/evaporative pellets if they are large and/or slow. For pellets whose neutral production is due to physical sputtering it seems unlikely that the disturbance would be substantial; even large surfaces such as limiters continuously in contact with the edge plasma generally do not disturb the plasma by impurity release. Quantitatively one may consider the example of $n_e = 10^{19}$ m^{-3}, $T_e = T_{D^+} = 50$ eV for which the D^+-D^+ mean free path $\lambda_{ii} \approx 3$ m. Even neglecting ion heat conduction across or along $\vec{B}$, the diluting effect on the local ion temperature, T_{D^+}, extending over a distance λ_{ii} from the injection along $\vec{B}$, will not be great since this length of flux tube contains an order of magnitude, or more, D^+ ions than the number of Li particles injected. With regard to disturbance to T_e, electron heat conduction along $\vec{B}$ would be sufficiently strong to prevent significant cooling; for the same example, and assuming a length of T_e-gradient along $\vec{B}$ of ~10 m (beyond which cross-field heat transfer is assumed to be strong enough to keep T_e fixed at 50 eV) then an impurity radiation load of ~10^3 eV/particle injected only reduces T_e by ~1 eV near the pellet.

When low signal levels are a problem then ablative/evaporative pellets may be required, providing they are kept small enough and/or fast enough to avoid plasma disturbance. The source particle release mechanisms may be simpler and better known *a priori* than for physical sputtering, thus permitting more reliable use of the neutral experimental data. The spatial extent of the neutrals, however, may be too small to be spatially resolved.

In practice it will be important to confirm that the plasma is not being changed locally. Varying the pellet size and speed should yield the same plasma parameters for identical plasma operating conditions until the pellet size is made too great or the speed too low.

General Procedure

The foregoing outline of the proposed procedures for obtaining the plasma parameters has placed emphasis on the possibilities of extracting each parameter separately and by simple, analytic methods. This was done primarily to demonstrate the principles involved and to indicate sensitivities. The more general procedure recommended would be to employ these techniques to obtain a first estimate of the parameters which would then be used to assist in the identification of a best-fit solution employing an impurity transport code such as LIM. In this way all of the experimental data would contribute to the identification of a set of plasma parameters. Generally it would be expected that a unique set of parameters would be obtained by this procedure since the number of measured quantities can readily be made sufficiently large to constrain the solution. The use of a code and a fitting procedure may also make it possible to deduce the cross-field diffusion coefficient if measurements of sufficiently long-lived states are made.

The cases analysed above assumed the existence of a known source mechanism, characterized by specific velocity and angular distributions of the released neutrals, e.g., v_0, etc. For the case of impurity injection via fast pellets, the source may be difficult to characterize in practice. Release may be due to a combination of sputtering, sublimation and other processes — each with their own neutral velocity distributions. Sputtering will be by plasma impurity ions, as well as hydrogenic ions, each process having a different velocity cut-off for the released neutrals. The pellet shape may change during flight and tumbling may occur, influencing the angular distribution of the neutrals. Such complications would not necessarily prevent the extraction of plasma parameters, however, the simple and one-step-at-a-time techniques described above would provide poorer first estimates, and a greater dependence on the use of an

impurity code to fit all of the available experimental data would be necessary. Some of the experimental data, which could otherwise have been used for consistency checks, would be required directly for extraction of the plasma parameters. For example, with the use of a code the measured neutral particle spatial distribution and the measured neutral temperature become, in effect, a replacement for the possibly unknown source angular and velocity distributions.

It is therefore worth considering alternative impurity injection methods such as the laser blow-off and neutral beam techniques employed on TEXTOR [3,4] to evaluate n_e and T_e from the spatial distribution of neutral impurity particles across $\vec{B}$. Since the presently proposed techniques are based, in part, on the spatial distributions of neutrals and ions along $\vec{B}$, it would be useful to have simple and well-characterized velocity distributions of the neutrals along $\vec{B}$ — which can be the case for these injection methods. The achievement of a narrow beam of impurities would be useful for the application of the simple approximate methods of parameter evaluation, which is more readily achieved with the neutral beams than laser blow-off. In any case, the beam width should not be substantially greater than the λ_{iz} values for the states of interest.

The viewing system in Fig. 1 need not involve time-resolution. Incorporation of time-resolution, however, would provide additional data which could be usefully employed in finding an over-all fit between experiment and (time-dependent) modelling to extract the plasma parameters. The time resolution would generally have to be quite fast in order to follow the low ionization states which peak quickly; for example, for carbon and T_e = 50 eV, $n_e = 10^{19}$ m^{-3} one has $\tau_0/\tau_1/\tau_2/\tau_3$ = 1.1/5.4/27/175 μs.Thus even with an image intensifier, it may not be possible to obtain time-resolved information for the lowest stages. Time-resolution for the lowest stages would also require high penetration velocities of the impurity beam (across $\vec{B}$): if a radial spatial resolution of 1 cm is wanted then a 10 μs time resolution requires a penetration velocity

$>10^3$ m/s. Such penetration velocities are at the limit of pellet technology, although they are achievable using the other methods.

Conclusion

A large number of plasma diagnostic possibilities would appear to exist, based on impurity injection with measurements of spatial profiles of successive charge states of the impurity and spectroscopic (Doppler) temperature measurements of the states. The use of an impurity pellet would enjoy advantages of simplicity, good penetration and flexibility as to impurity type. A number of potential concerns will require experimental resolution including adequate viewing, adequate signal, avoidance of plasma disturbance and uncertainties associated with the velocity and angular distribution of the impurity neutrals. As a first approximation, it should be possible to extract plasma parameters from the experimental data by one-step-at-a-time procedures based on simple analytic formulae. In practrice, given various uncertainties, particularly those related to the particle source mechanisms, it will be necessary to employ an impurity transport code such as LIM with the plasma input parameters varied so as to obtain the best fit to all of the experimental data simultaneously.

Acknowledgement

The authors wish to thank G. Janeschitz, Guy Matthews, Garry McCracken, Spencer Pitcher and Peter Stott for helpful discussions. Support by the Canadian Fusion Fuels Technology Project is acknowledged.

References

1. G. M. McCracken, U. Samm, S. J. Fielding, et al, "A Study of Impurity Transport in the Plasma Boundary of TEXTOR Using Gas Puffing", Proc. 9th Int. Conf. Plasma Surface Interactions, Bournemouth, U.K., May 1990. To be published in J. Nucl. Mater.
2. S. J. Fielding, G. M. McCracken, R. A. Pitts, et al, Proc. 17th EPS Conf. on Controlled Fusion and Plasma Heating, Amsterdam, June 1990, 14B, p. 1472.
3. P. Bogen and E. Hintz in Physics of Plasma-Wall Interactions in Controlled Fusion (Proc. NATO Advanced Study Institute Val-Morin, Quebec, 1984), NATO ASI Series, Vol. 131, Plenum Press, New York (1986), 211.
4. A. Pospieszczyk and G. G. Ross, Rev. Sci. Instrum. 59 (1988), 1491.
5. J. L. Terry, E. S. Marmar, J. A. Snipes (MIT Li Pellet Experiment on TFTR), to be published.
6. P. C. Stangeby, "Impurity Transport at the Plasma Edge", Proc. 9th Int. Conf. on Plasma Surface Interactions, Bournemouth, U.K., May 1990, To be published in J. Nucl. Mater.
7. P. C. Stangeby, C. Farrell, S. Hoskins, et al, Nucl. Fusion 28 (1988), 1945.
8. P. C. Stangeby and C. Farrell, Plasma Phys. and Controlled Fusion 32 (1990) 677.
9. M. W. Thompson, Phil. Mag. 18 (1968), 377.
10. J. Bohdansky (1984) Special Issue of Nuclear Fusion, p. 61.
11. A. Pospieszczyk, F. Aumayr, H. L. Bay, et al, J. Nucl. Mater. 162-164 (1989) 574.
12. P. C. Stangeby, Contrib. Plasma Phys. 28 (1988), 507.
13. R. R. Weynants and R. J. Taylor, Nucl. Fusion 30 (1990), 945.

References

Bogen, P., and Hintz, E., in Physics of Plasma-Wall Interactions in Controlled Fusion (Proc. NATO Advanced Study Institute Val-Morin, Quebec, 1984), NATO ASI Series, Vol. 131, Plenum Press, New York (1986), 211.

Bohdansky, J. (1984) Special Issue of Nuclear Fusion, p. 61.

Fielding, S. J., McCracken, G. M., Pitts, R. A., et al, Proc. 17th EPS Conf. on Controlled Fusion and Plasma Heating, Amsterdam, June 1990, 14B, p. 1472.

McCracken, G. M., Samm, U., Fielding, S. J., et al, "A Study of Impurity Transport in the Plasma Boundary of TEXTOR Using Gas Puffing", Proc. 9th Int. Conf. Plasma Surface Interactions, Bournemouth, U.K., May 1990. To be published in J. Nucl. Mater.

Pospieszczyk, A., and Ross, G. G., Rev. Sci. Instrum. 59 (1988), 1491.

Pospieszczyk, A., Aumayr, F., Bay, H. L., et al, J. Nucl. Mater. 162-164 (1989) 574.

Stangeby, P. C., Farrell, C., Hoskins, S., et al, Nucl. Fusion 28 (1988), 1945.

Stangeby, P. C., Contrib. Plasma Phys. 28 (1988), 507.

Stangeby, P. C., and Farrell, C., Plasma Phys. and Controlled Fusion 32 (1990) 677.

Stangeby, P. C., "Impurity Transport at the Plasma Edge", Proc. 9th Int. Conf. on Plasma Surface Interactions, Bournemouth, U.K., May 1990, J. Nucl. Mater. 176&177 (1990), 51.

Terry, J. L., Marmar, E. S., Snipes, J. A. (MIT Li Pellet Experiment on TFTR), to be published.

Thompson, M. W., Phil. Mag. 18 (1968), 377.

Weynants, R. R., and Taylor, R. J., Nucl. Fusion 30 (1990), 945.

Table 1

Extraction of n_e and T_e from spatial distribution of impurities as calculated by the LIM impurity transport code. λ_q is the average ionization mean-free-path for ion of charge q. The LIM value of λ_q is the e-folding length of the LIM-calculated spatial profile. The $v_o\tau_q$ value is the λ_q value simply calculated from the original neutral velocity v_o (for 15 eV) and the mean ionization time τ_q. The values of n_e and T_e are then calculated from the LIM values of λ_q: the n_e value deduced from λ_{Lio} assumed $\overline{\sigma v}_{iz} = 8.5\times10^{-14}\ m^{-3}\ s^{-1}$ for all cases; the T_e values were obtained from the theoretical curves, Fig. 3.

Impurity	Input to LIM Code				λ_o		λ_1		λ_2		n_e and T_e deduced from LIM output						
												T_e [eV] from:					
	T_e [eV]	T_{D+} [eV]	n_e [10^{18} m^{-3}]	Z_{eff}	LIM [mm]	$v_o\tau_o$ [mm]	LIM [mm]	$v_o\tau_1$ [mm]	LIM [m]	$v_o\tau_2$ [m]	n_e [10^{19} m^{-3}]	$\lambda_{C+}/\lambda_{Lio}$	$\lambda_{C2+}/\lambda_{Lio}$	$\lambda_{Li+}/\lambda_{Lio}$	$\lambda_{C+}/\lambda_{Co}$	$\lambda_{C2+}/\lambda_{C+}$	$\lambda_{Li+}/\lambda_{C+}$
Carbon	100	100	10	1	14	14	60	56	0.28	0.28		93	90		85	82	
	50	50	10	1	18	18	84	82	0.41	0.49		45	53		43	76	
	25	25	10	1	27	27	150	176	0.92	1.43		24	30		23	43	
	50	50	10	3	18	18	80	82	0.61	0.49		47	39		75	34	
	50	100	10	1	18	18	84	82	0.44	0.49		45	51		37	57	
	50	25	10	1	18	18	80	82	0.61	0.49		47	39		50	34	
	50	50	2	1	87	87	400	420									
							[m]	[m]									
Lithium	100	100	10	1	27	27	0.94	1.12			0.88			120			145
	50	50	10	1	23	23	3.2	3.1			1.03			50			55
	25	25	10	1	23	23	5.1	19			1.03						60
	50	50	10	3	23	23	2.9	3.1			1.03			55			57
	50	100	10	1	23	23	2.0	3.1			1.03			67			88
	50	25	10	1	23	23	23	3.1			1.03			64			70
	50	50	2	1	111	113					0.21						

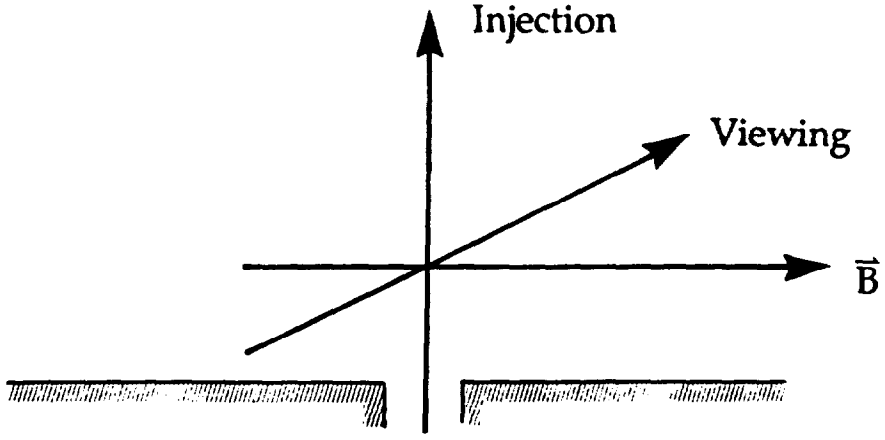

Figure 1. Schematic of ideal injection and viewing arrangement. View to measure impurity density and impurity temperature of successive charge states two-dimensionally, along $\vec{B}$ and along the line of injection.

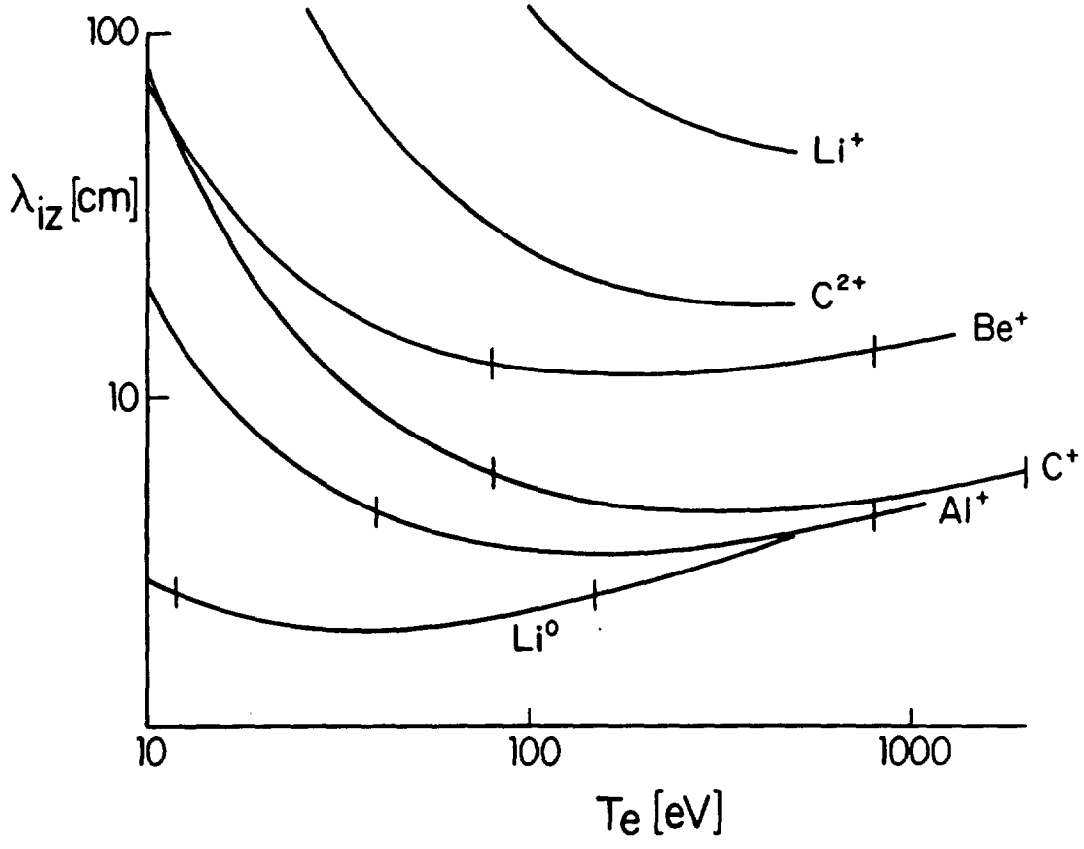

Figure 2. Mean-free-path for ionization λ_{iz} for particles moving with 15 eV kinetic energy as a function of T_e; $n_e = 10^{19}$ m^{-3}. For certain species, such as Li^0, λ_{iz} is essentially constant over a wide range of T_e. The value of n_e can therefore be deduced from a measurement of λ_{iz}. The vertical bars marked on certain of the curves indicate the T_e-range over which λ_{iz} varies by less than ±10%.

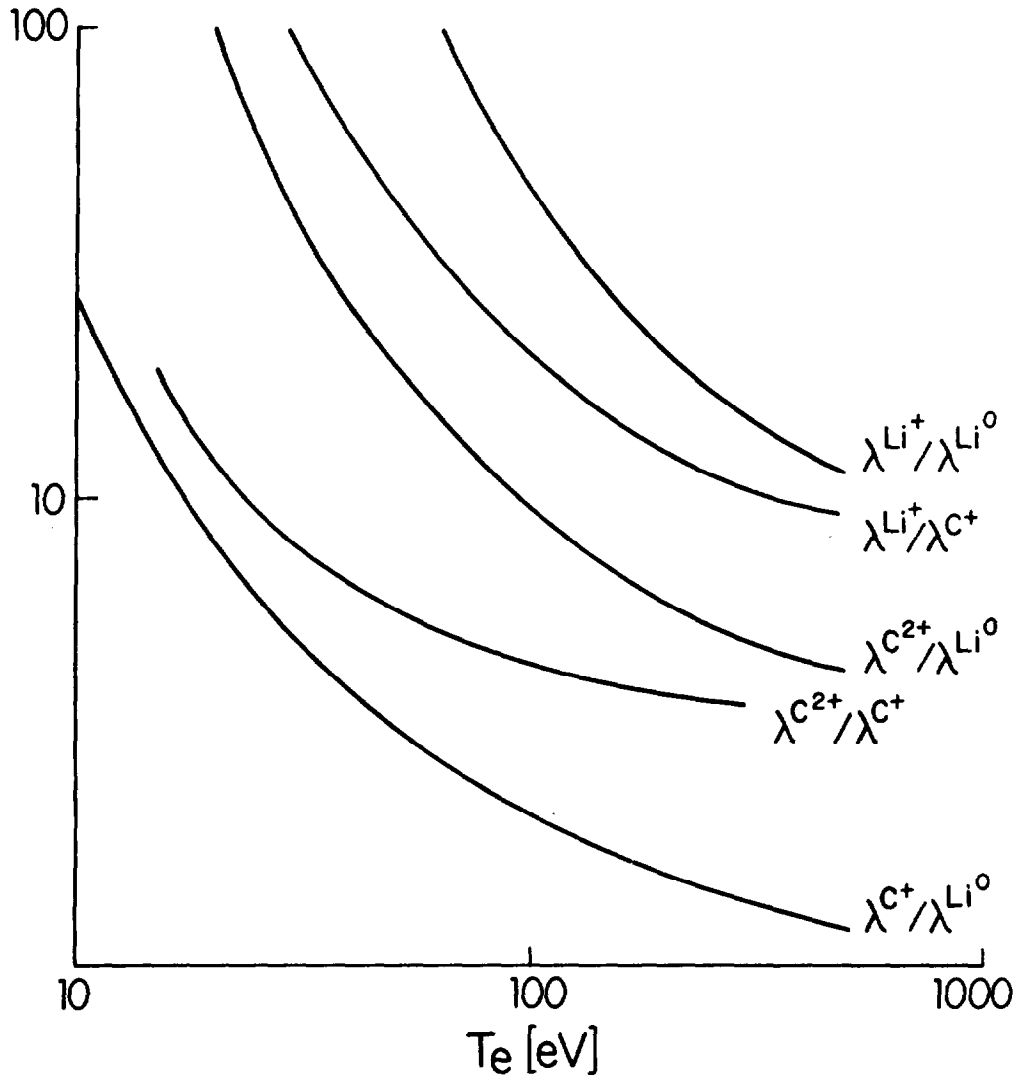

Figure 3. Ratio of λ_{iz} values for various pairs of impurity species. Ratios are independent of n_e therefore providing a means of measuring T_e. Generally it is possible to find a species pair for which reasonable sensitivity occurs, i.e., about a factor 2 change in the ratio for a change of factor 2 in T_e.

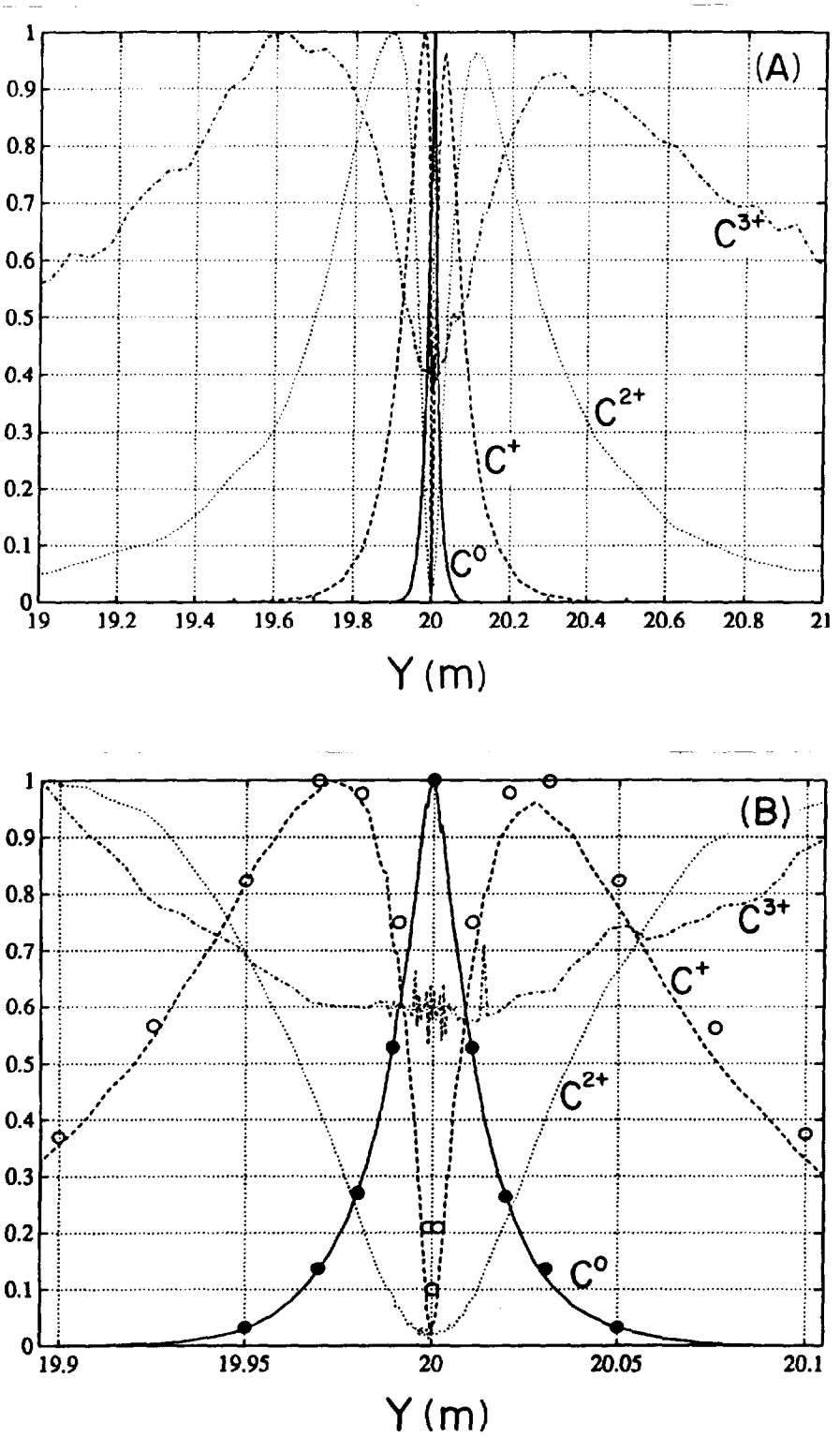

Figure 4. LIM-calculated profiles of C^0, C^+, C^{2+}, C^{3+} for injection of 15 eV neutrals in the region y ε [19.002, 20.002 m] (lines). Case of $T_e = T_{D+} =$ 100 eV, $n_e = 10^{19}$ m^{-3}, $Z_{eff} = 1$, no deuterium flow velocity. The points are from the analytic expressions, Eqs. (1), (2). B gives expanded view of A.

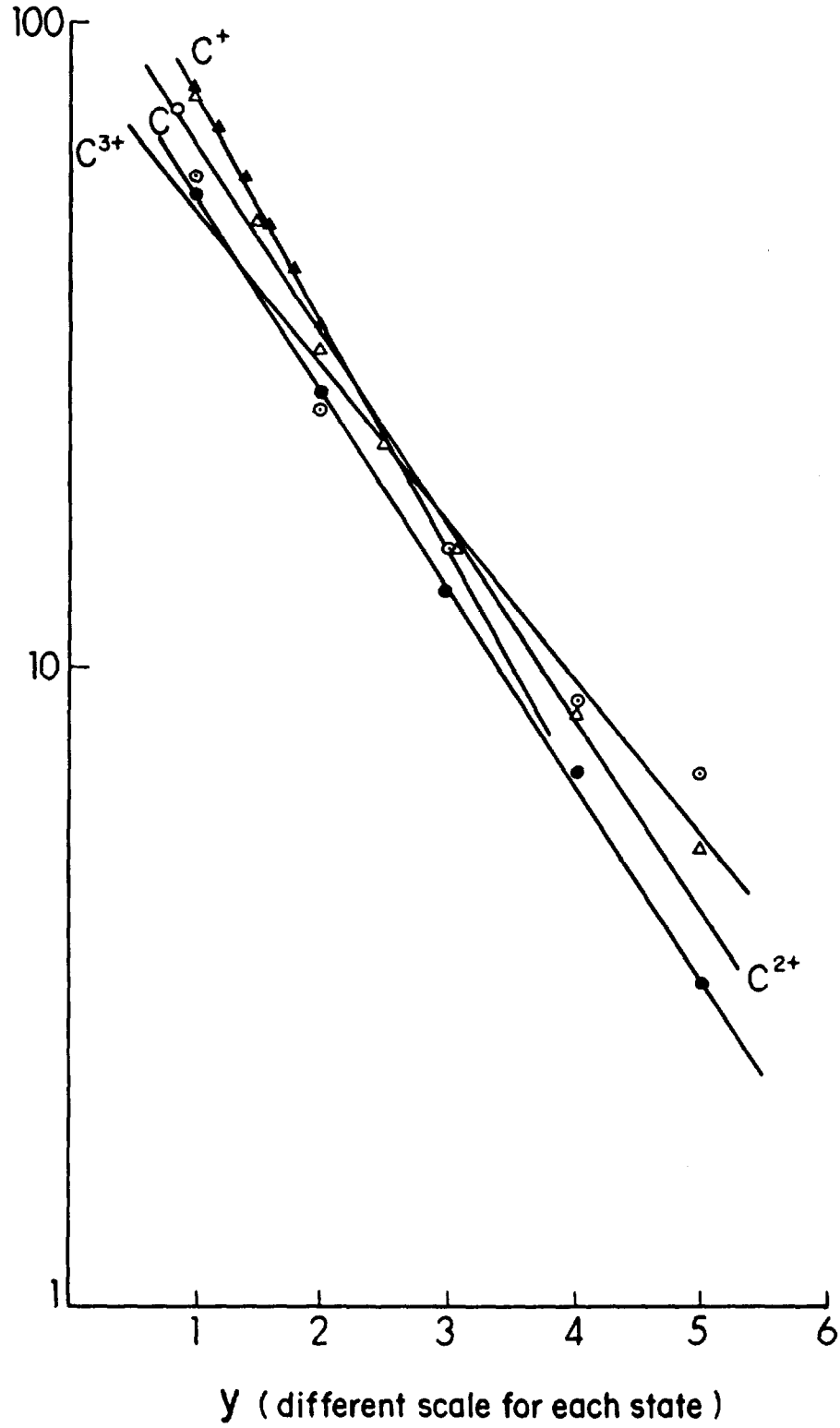

Figure 5. Logarithmic plots of C^0, C^+, C^{2+}, C^{3+} profiles shown in Fig. 4. C^0 (●), C^+ (▲), C^{2+} (Δ), C^{3+} (⊙). Profiles are seen to be approximately exponential but for the higher ionization states the e-folding lengths differ from those simply-calculated, see text. Vertical scale is arbitrary. Horizontal scale differs for each state.

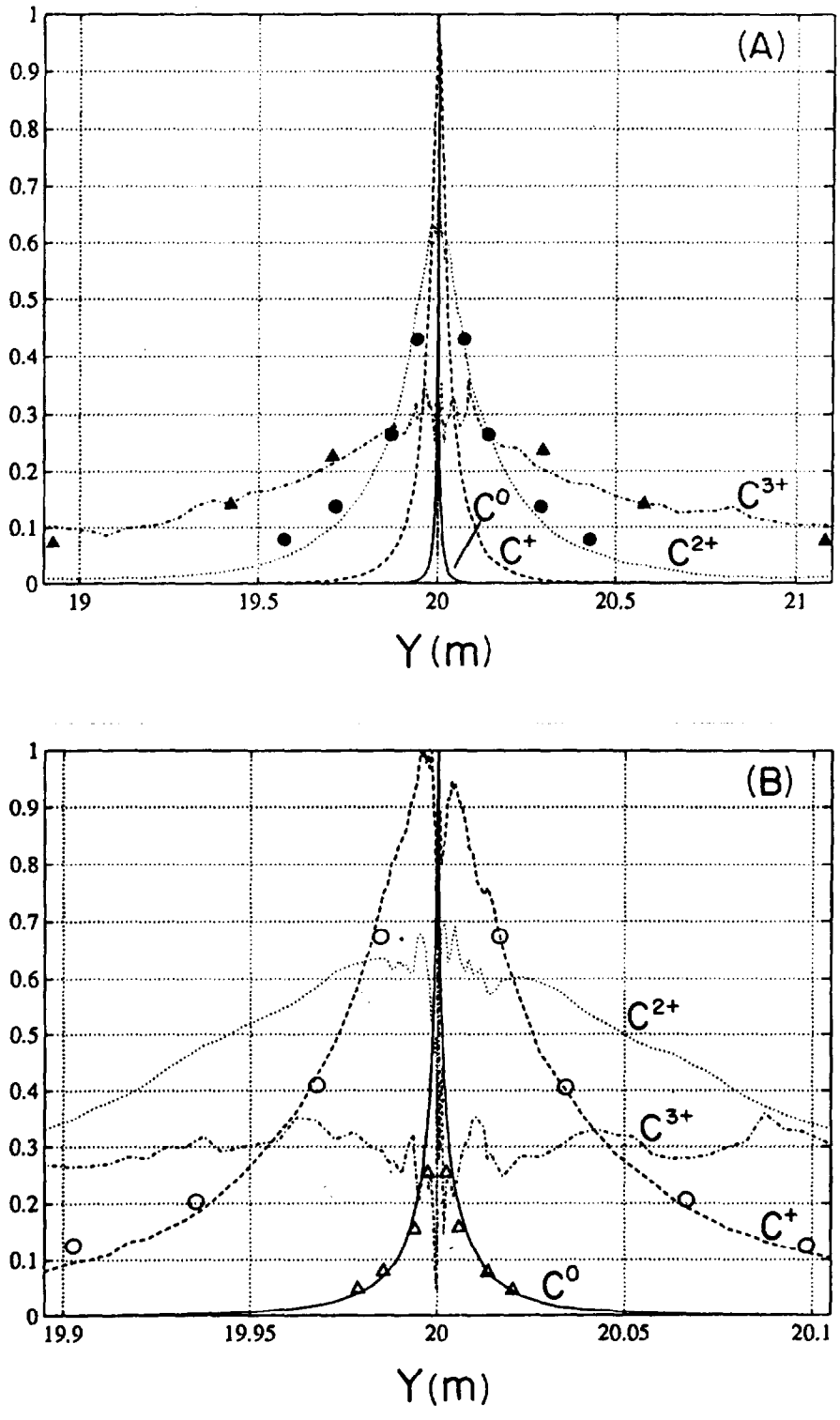

Figure 6. As for Fig. 4 but source is now characterized by a Thompson velocity distribution (with cut-off at maximum neutral energy) and an isotropic angular distribution. Lines give LIM code results, points from analytic expression, Eq. (3).

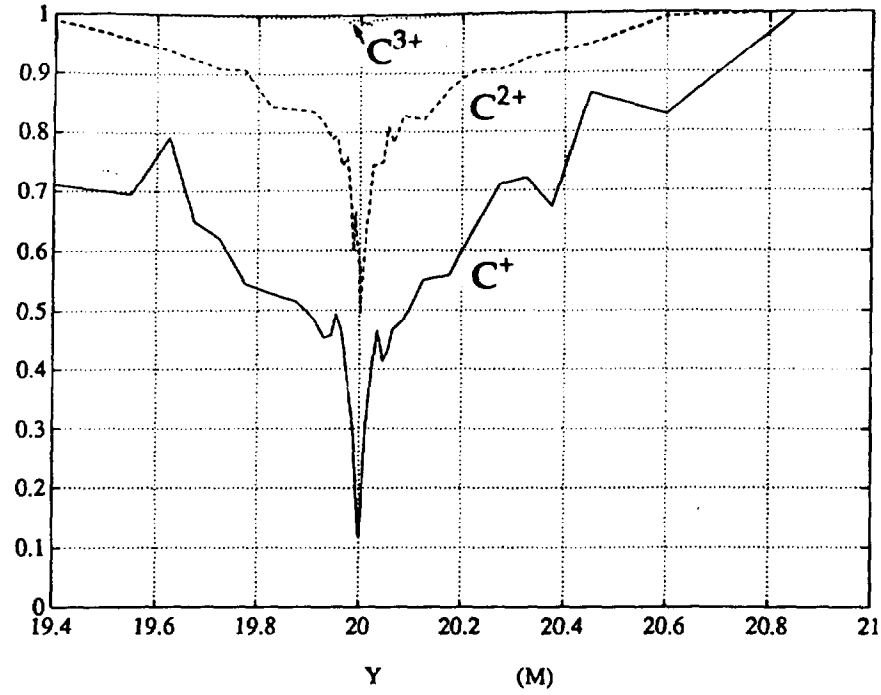

Figure 7a. Spatial variation of carbon ion temperatures calculated with the LIM impurity transport code. For $n_e = 2\times10^{19}$ m^{-3}, $T_e = 20$ eV, $T_{D+} = 40$ eV, $Z_{eff} = 1$, $v_{D+} = 0$, $D_\perp = 0$. Full scale: For C^+, 17.4 eV; for C^{2+}, 37.2 eV, for C^{3+}, 38.2 eV. The C^{2+}, C^{3+} have approximately thermalized to the local deuterium ion temperature within a short distance from the injection point at Y = 20 m. Source is 0.25 eV, isotropic atoms.

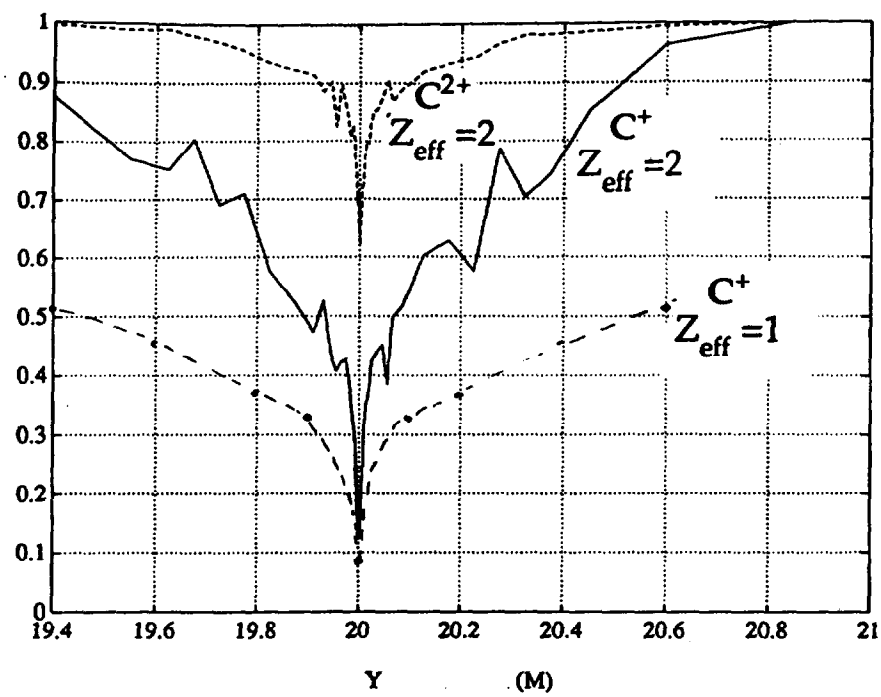

Figure 7b. Same as Figure 7a except $Z_{eff} = 2$. Full scale: for C^+, 26.6 eV; for C^{2+}, 38.1 eV; for C^{3+} 38.2 eV. For direct comparison, the C^{2+} curve from Figure 7a has been sketched in (same scale for the two C^+ curves).

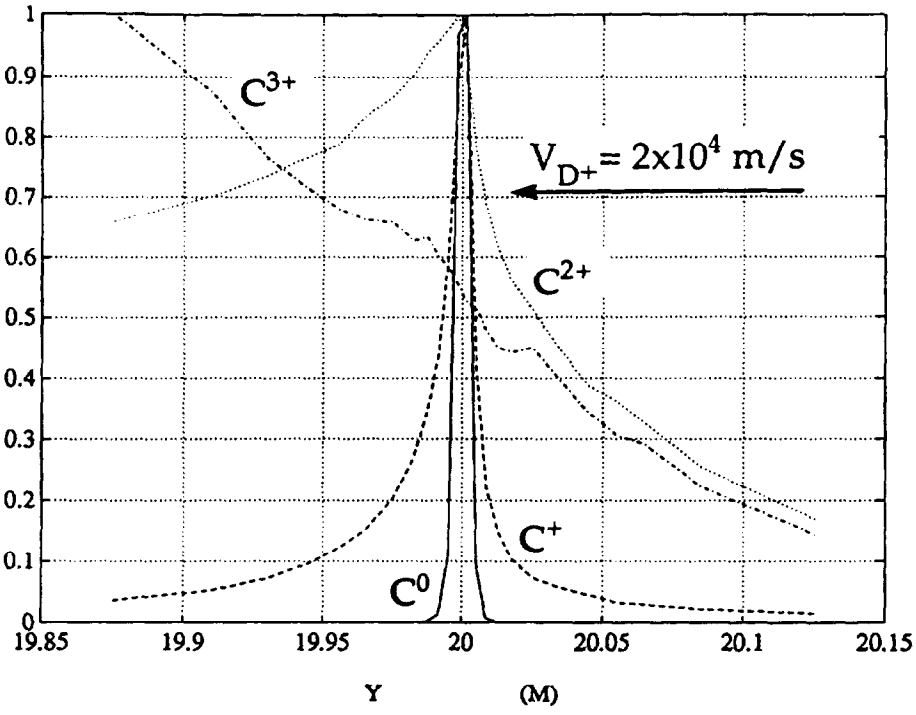

Figure 8. Carbon spatial profiles in a drifting deuterium plasma, $v_{D+} = 2\times10^4$ m/s to the left and purely along $\vec{B}$ (no poloidal drifts). $T_e = 20$ eV, $n_e = 2\times10^{19}$ m^{-3}, $T_{D+} = 20$ eV, $Z_{eff} = 1$, $D_\perp = 0$. Source is 0.25 eV, isotropic atoms.

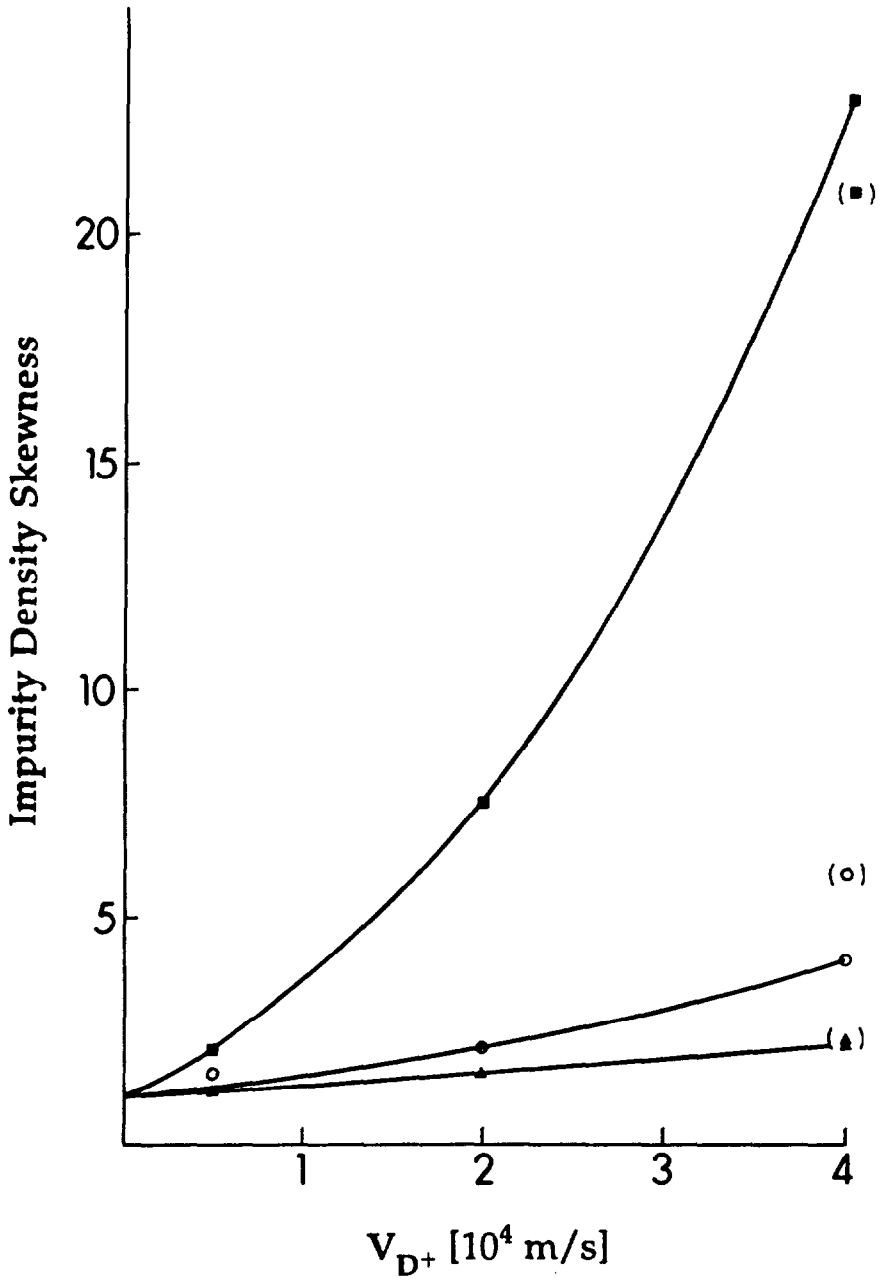

Figure 9. Dependence of skewness of C^{2+} and Fe^{2+} profiles as a function of v_{D+} and T_{D+}. Skewness ≡ ratio of densities of Z = 2 ions at locations ±5 cm either side of the injection point. For $n_e = 2 \times 10^{19}$ m^{-3}, T_e = 20 eV, Z_{eff} = 1. Results are for: T_{D+} = 10 eV, (■), 20 eV (○), 40 eV (▲). Bracketed points are for iron, other points for carbon. Carbon source is 0.25 eV neutrals, iron 1 eV neutrals. For reference it may be noted that the deuterium isothermal ion acoustic speed is 3.3×10^4, 4.4×10^4, 5.3×10^4 m/s for T_{D+} = 10, 20, 40 eV, respectively.

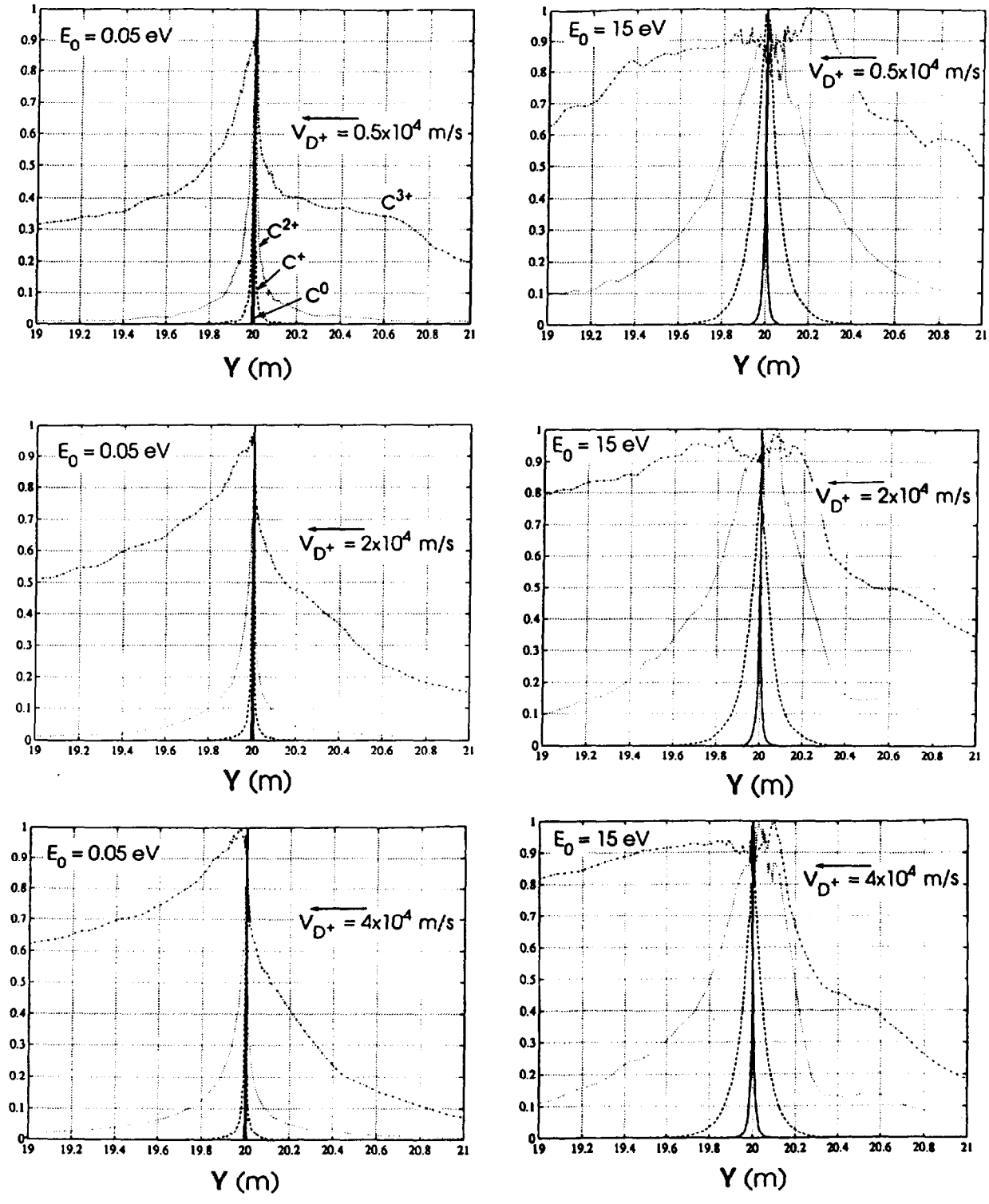

Figure 10. As Figure 8, but for a less collisional plasma. Here $T_e = T_{D+} = 50$ eV, $n_e = 10^{19}$ m^{-3}, $Z_{eff} = 1$, $D_\perp = 0$. Profiles are strongly dependent on the neutral launch energy, here 0.05 eV (as from dissociation of CO) and 15 eV (as from physical sputtering), however the sensitivity to deuterium drift velocity v_{D+} is about the same. The deuterium ion acoustic speed is 6.9×10^4 m/s.

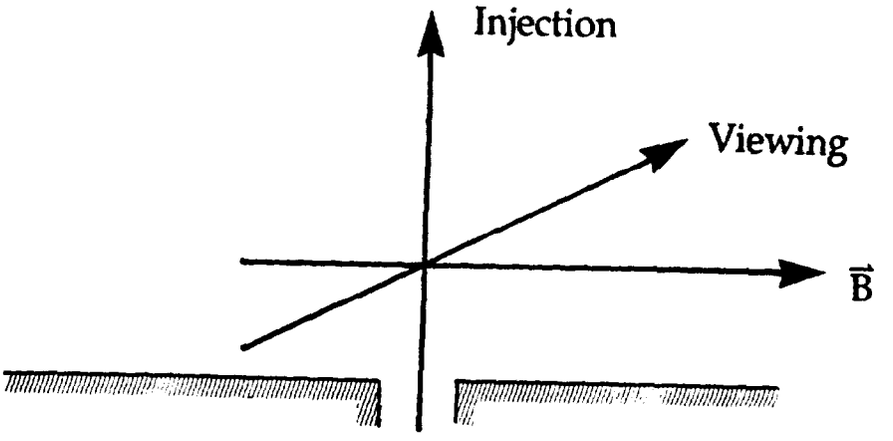

Fig 1

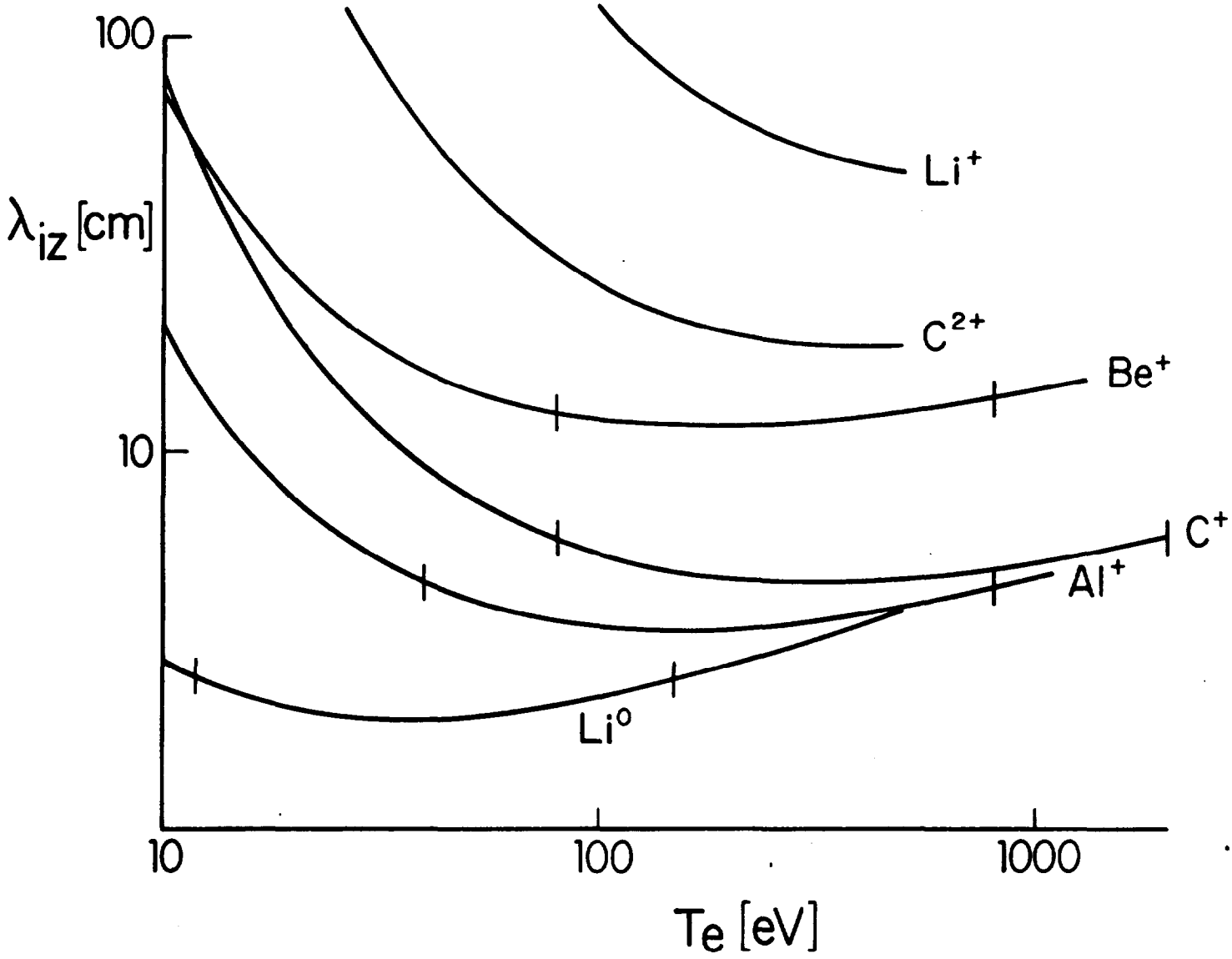

Fig 2

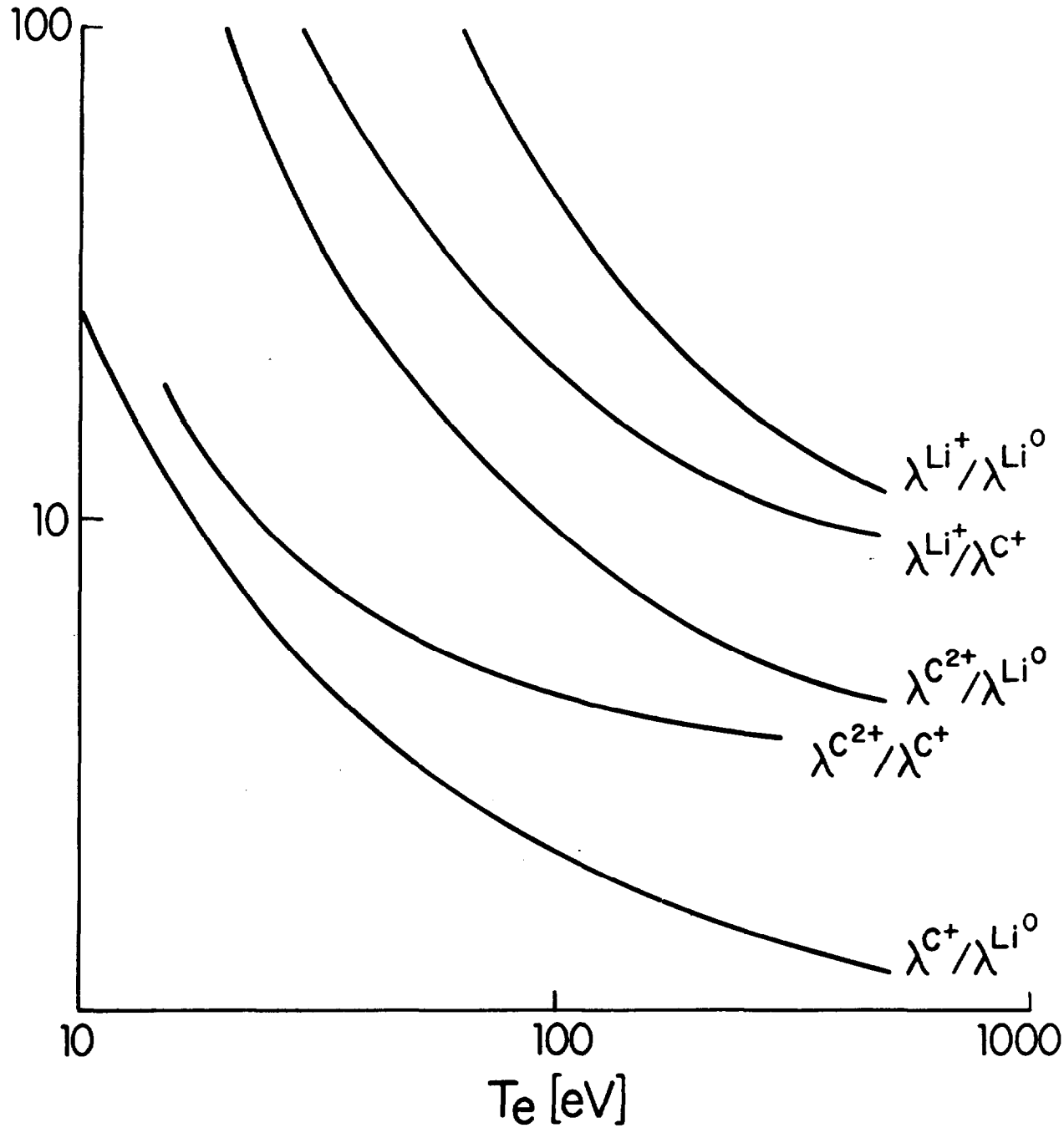

Fig 3

19.9 19.95 20 20.05 20.1

Y (m)

Fig 4A,B

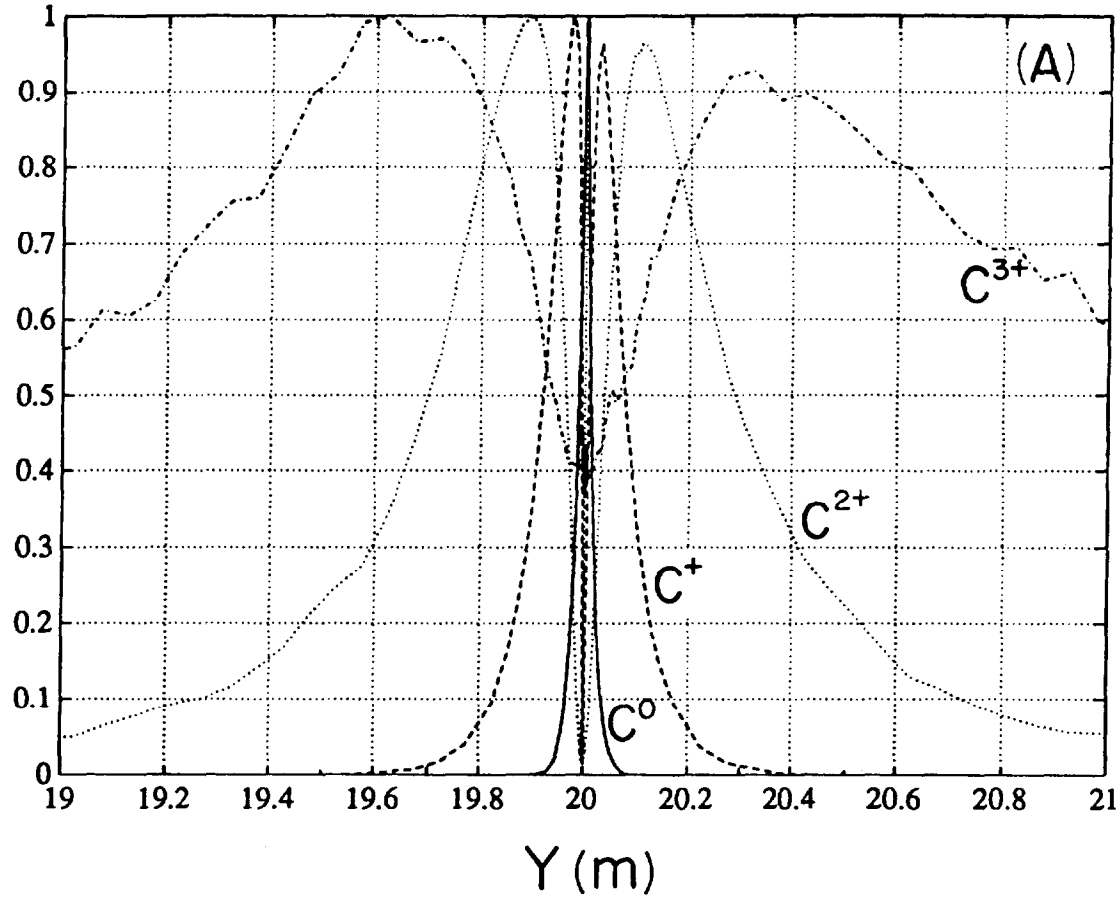

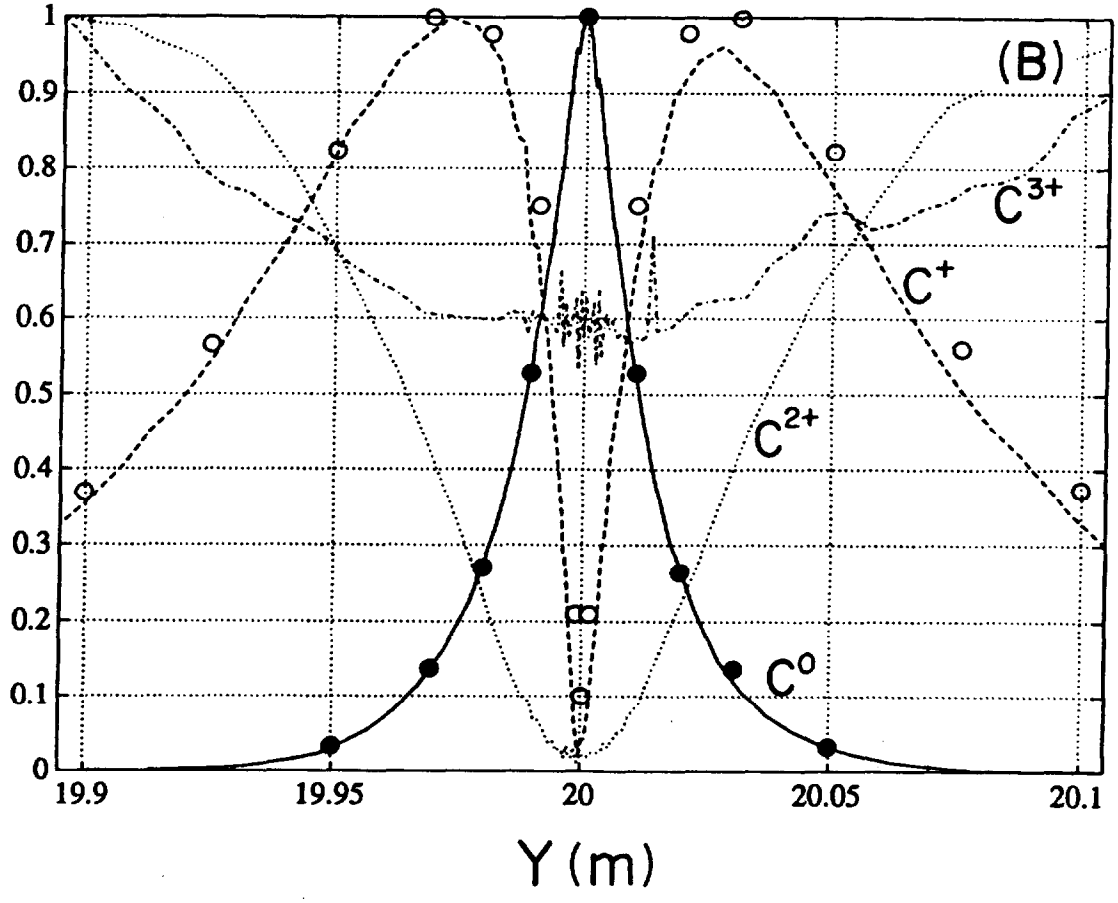

fig 5

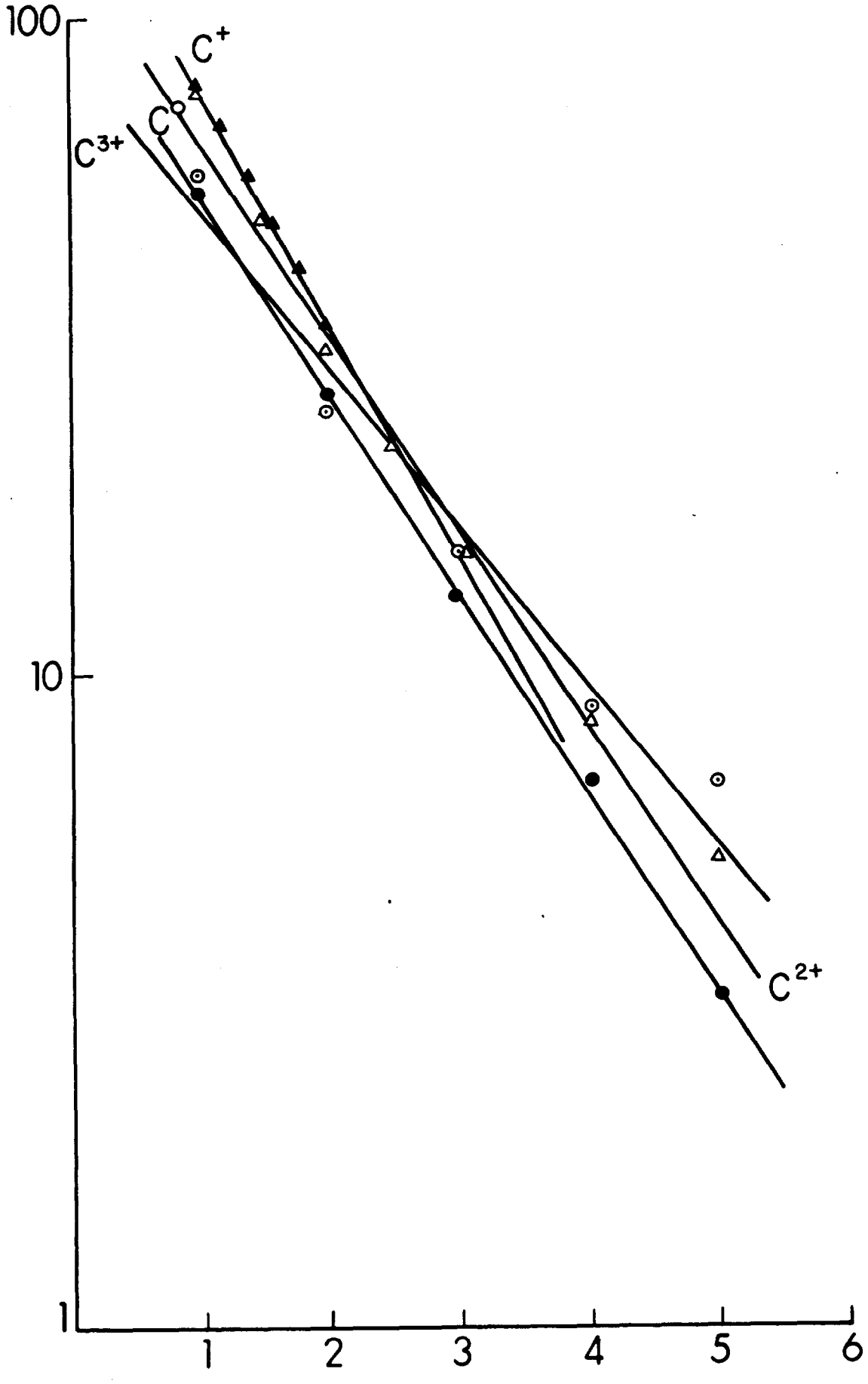

Fig 6A, B

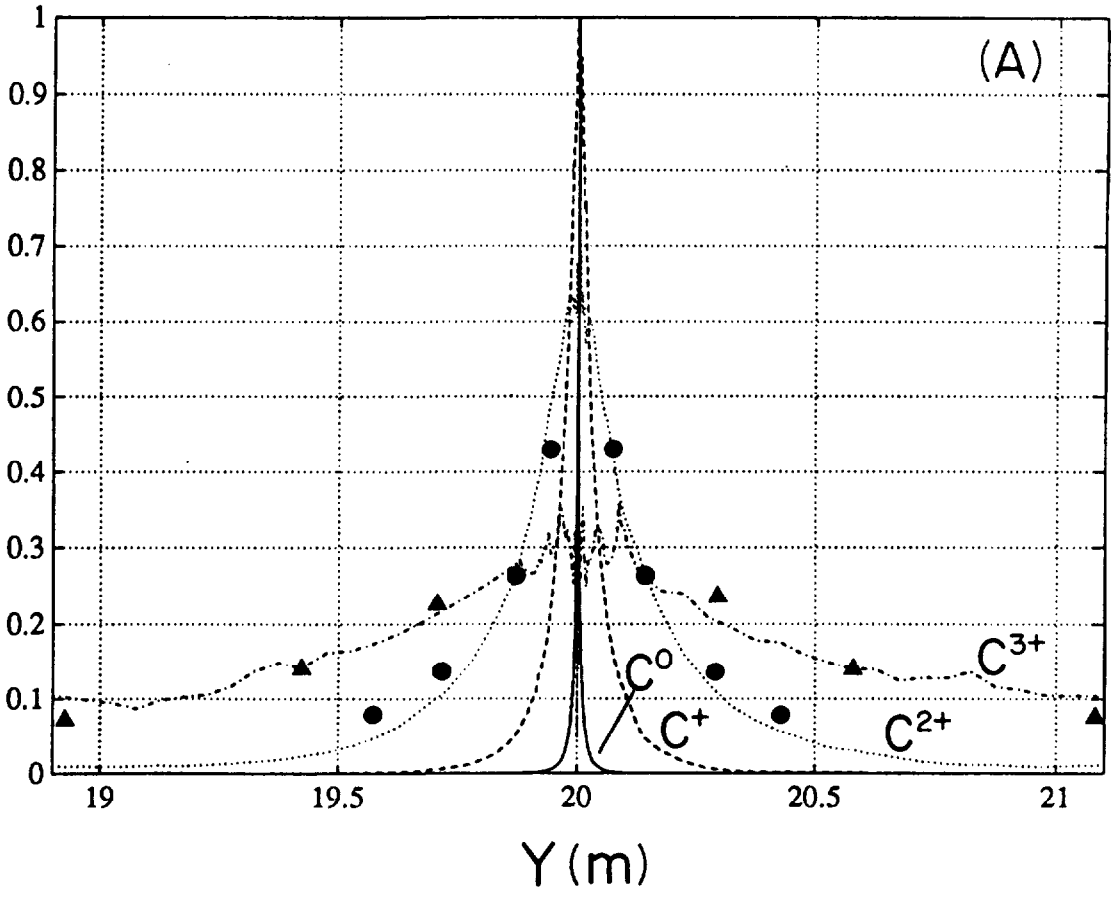
(A)
1
0.9
0.8
0.7
0.6
0.5
0.4
0.3
0.2
0.1
0
19
19.5
20
20.5
21
Y(m)
C⁰
C⁺
C²⁺
C³⁺

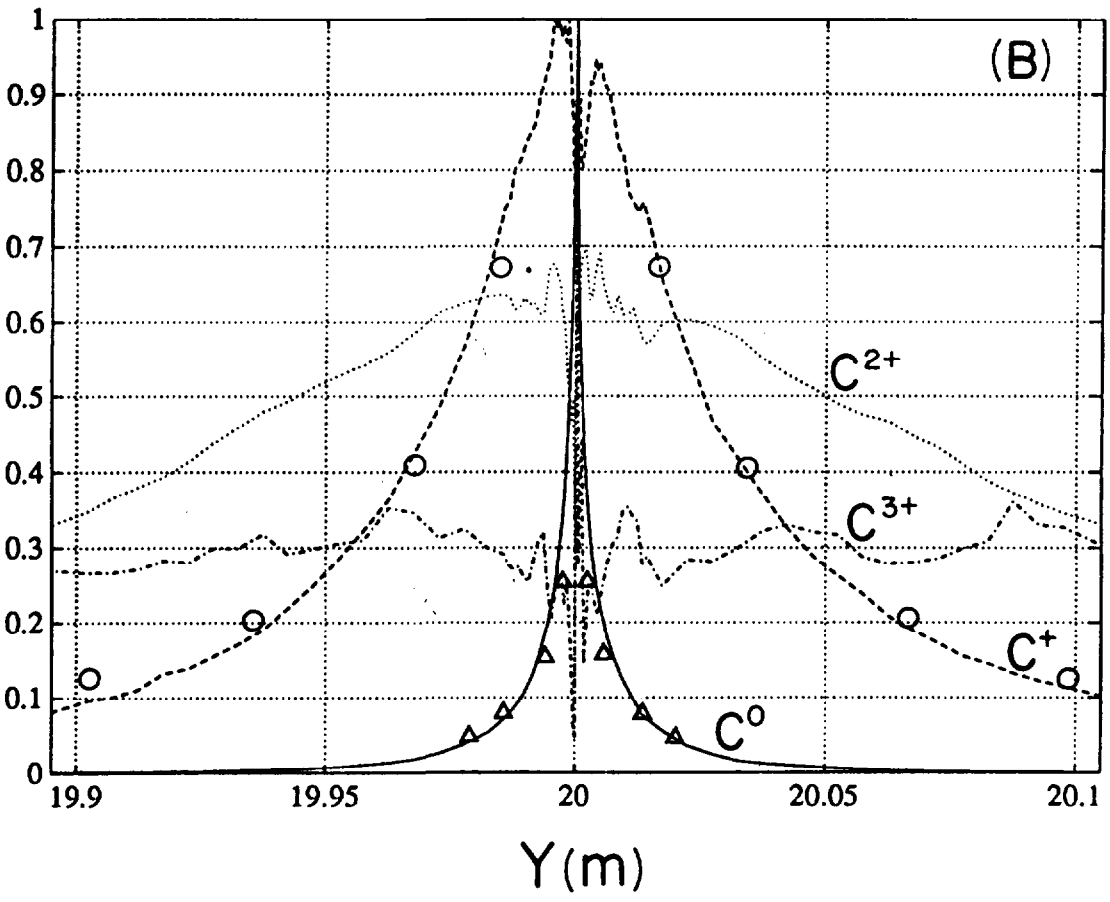
(B)
1
0.9
0.8
0.7
0.6
0.5
0.4
0.3
0.2
0.1
0
19.9
19.95
20
20.05
20.1
Y(m)
C²⁺
C³⁺
C⁺
C⁰

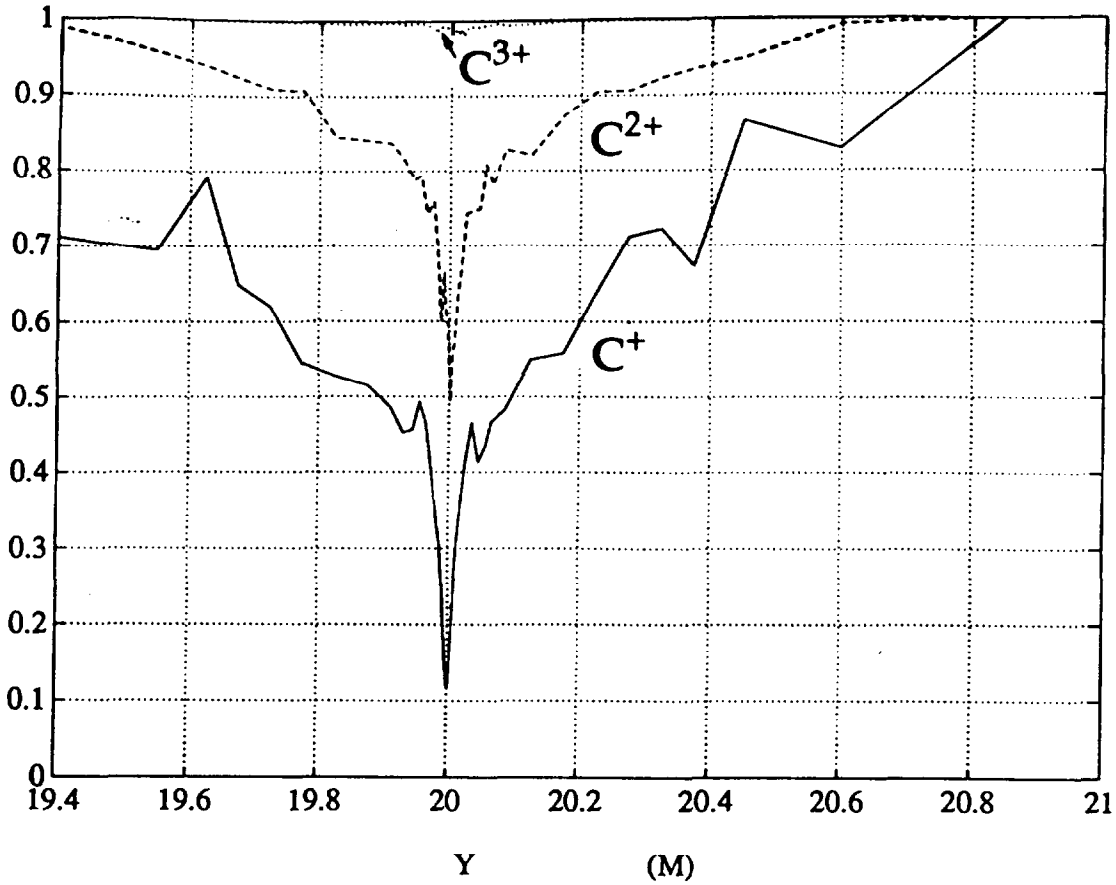
C3+
C2+
C+
1
0.9
0.8
0.7
0.6
0.5
0.4
0.3
0.2
0.1
0
19.4
19.6
19.8
20
20.2
20.4
20.6
20.8
21
Y (M)

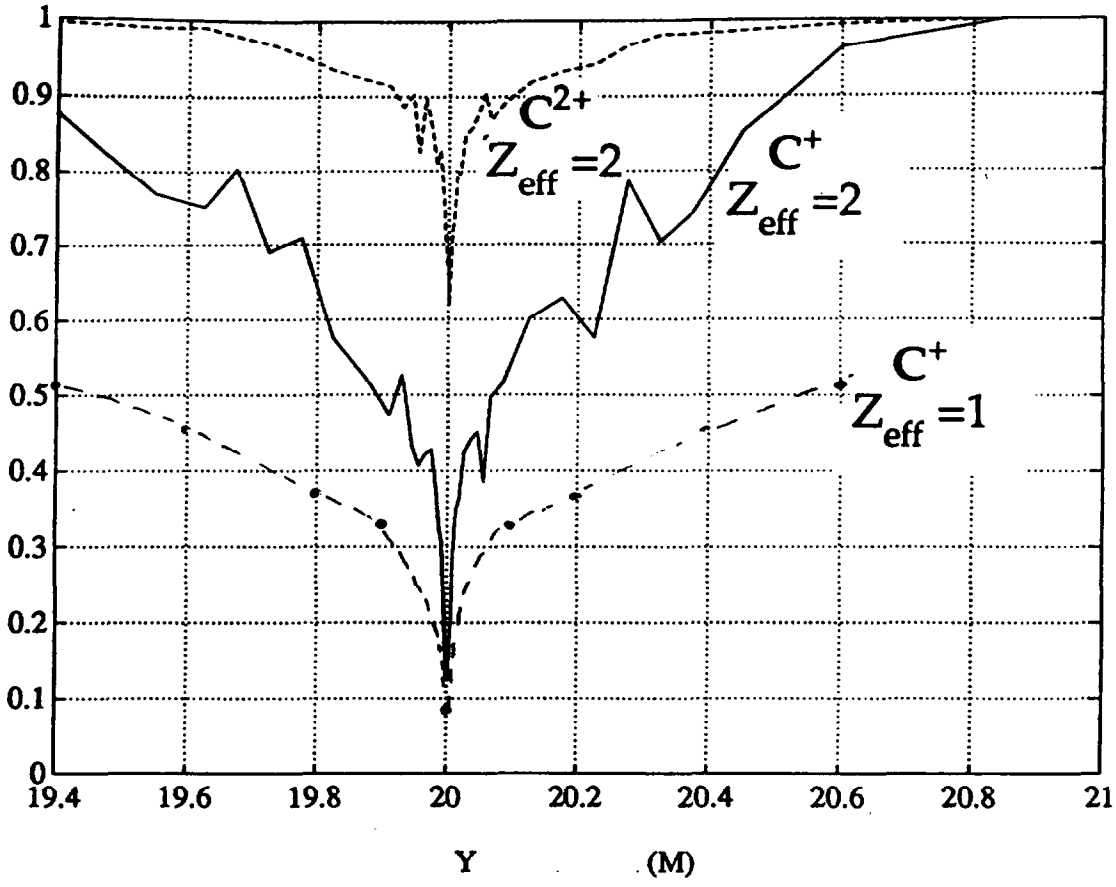
C2+
Zeff =2
C+
Zeff =2
C+
Zeff =1
1
0.9
0.8
0.7
0.6
0.5
0.4
0.3
0.2
0.1
0
19.4
19.6
19.8
20
20.2
20.4
20.6
20.8
21
Y (M)

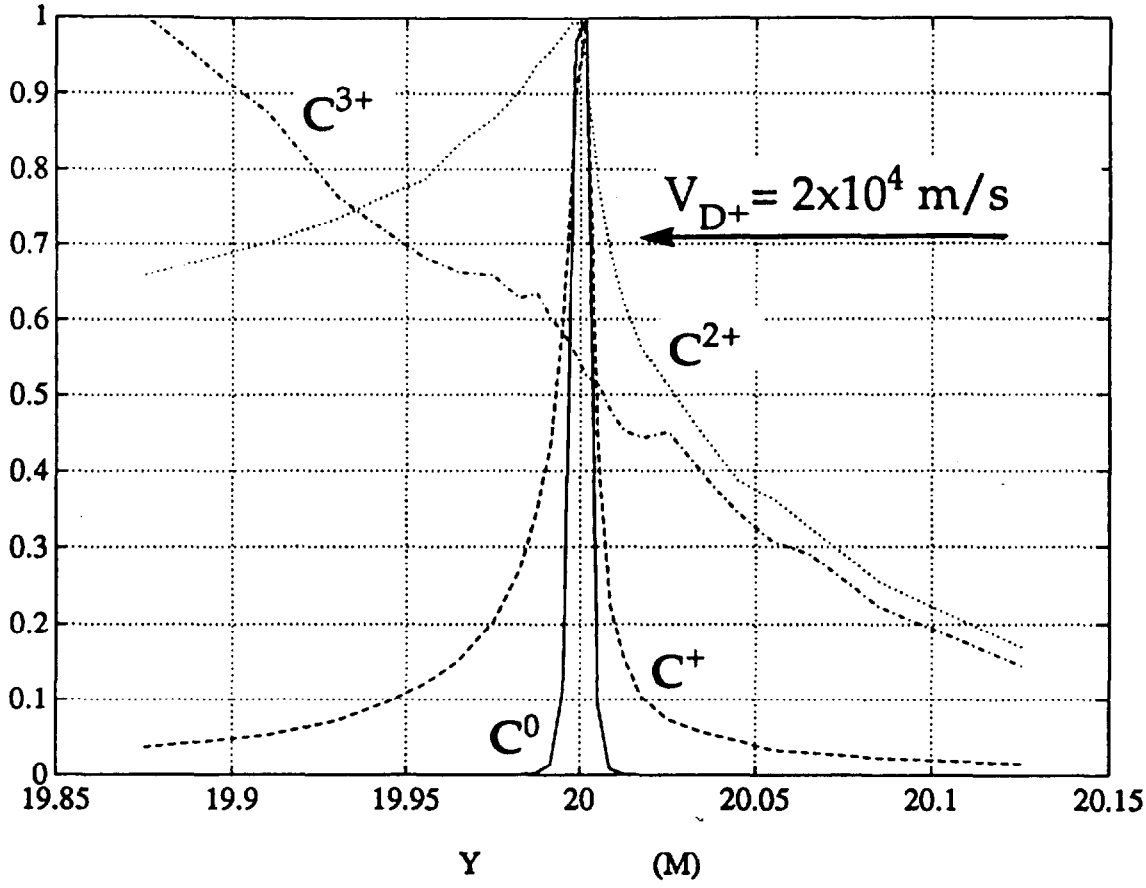
1
0.9
0.8
0.7
0.6
0.5
0.4
0.3
0.2
0.1
0
19.85
19.9
19.95
20
20.05
20.1
20.15
Y
(M)
C3+
C2+
C+
C0
VD+= 2x10^4 m/s

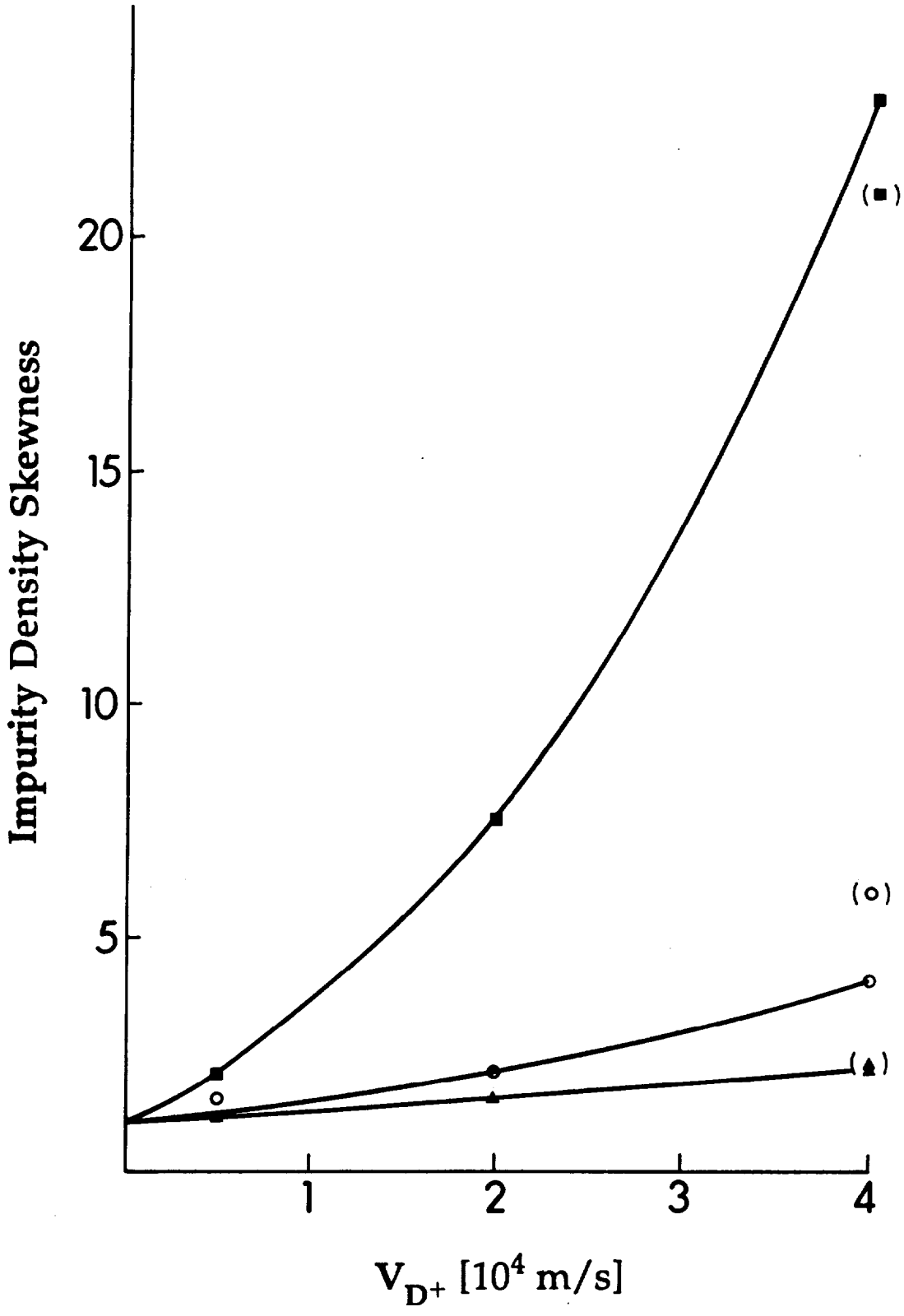

Fig 9

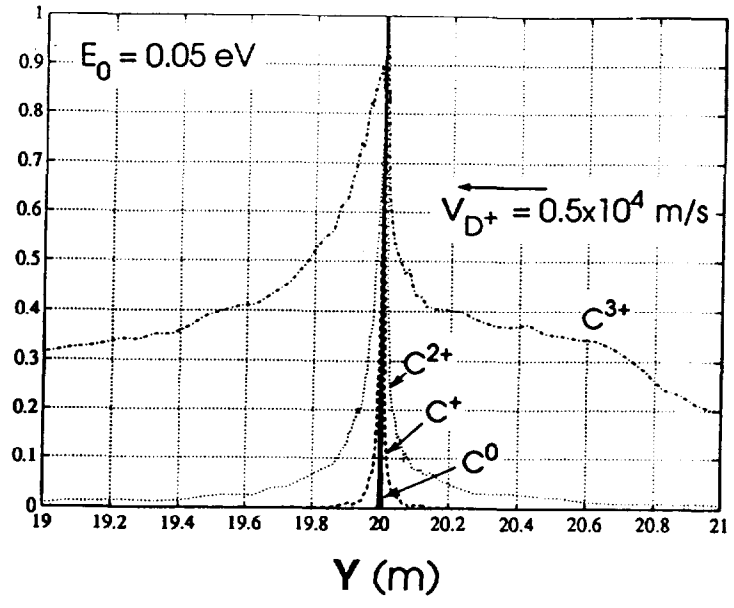
E_0 = 0.05 eV
V_{D^+} = 0.5x10^4 m/s
C^{3+}
C^{2+}
C^+
C^0
Y (m)

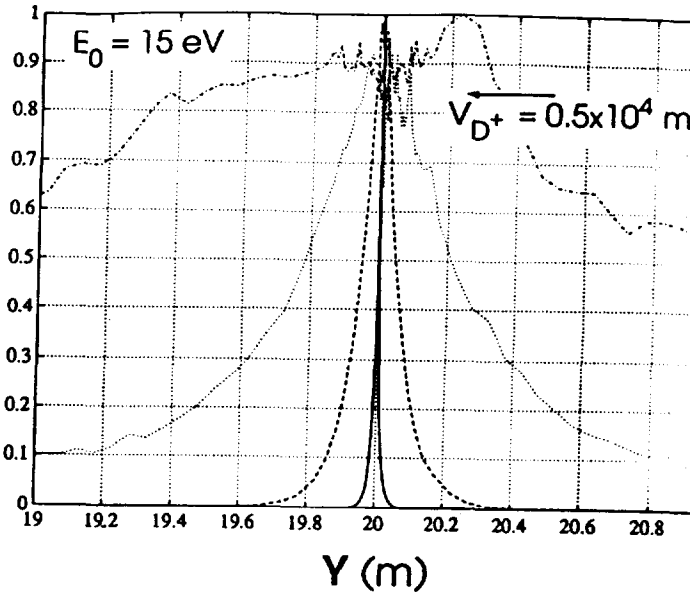
E_0 = 15 eV
V_{D^+} = 0.5x10^4 m
Y (m)

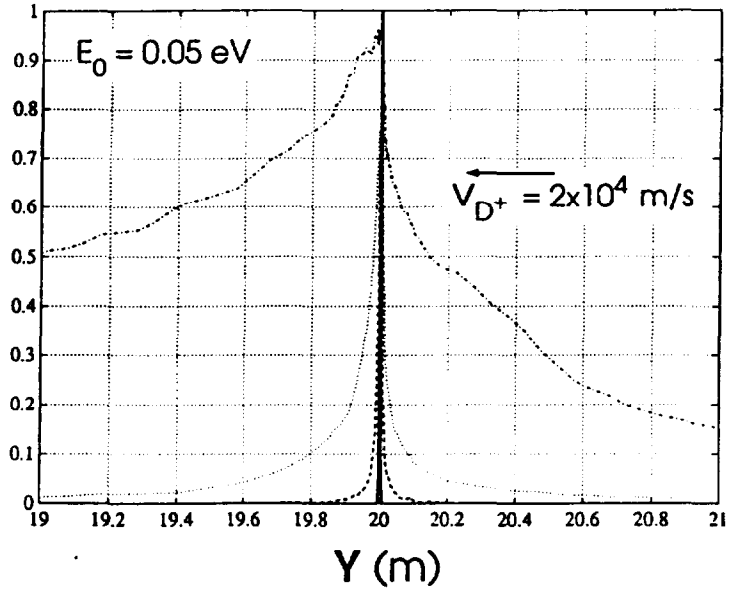
E_0 = 0.05 eV
V_{D^+} = 2x10^4 m/s
Y (m)

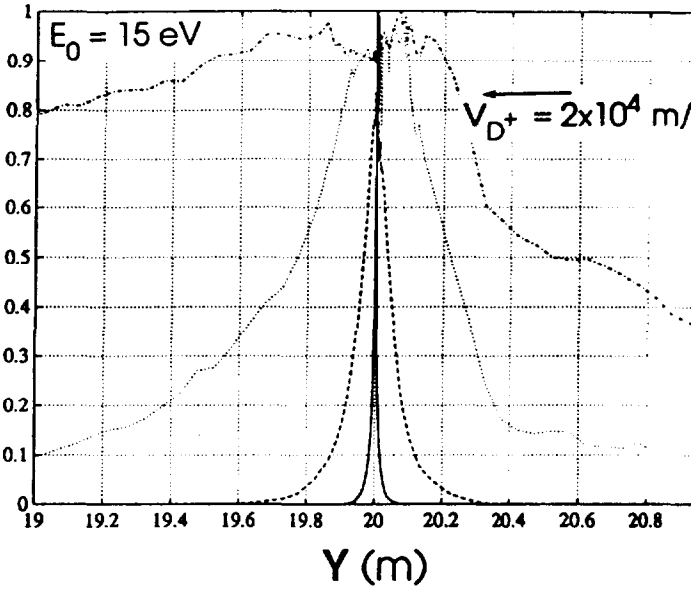
E_0 = 15 eV
V_{D^+} = 2x10^4 m/
Y (m)

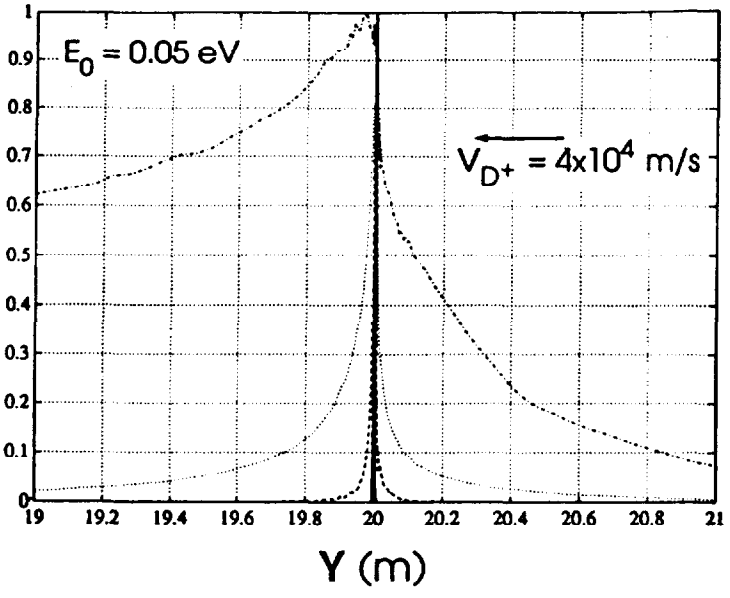
E_0 = 0.05 eV
V_{D^+} = 4x10^4 m/s
Y (m)

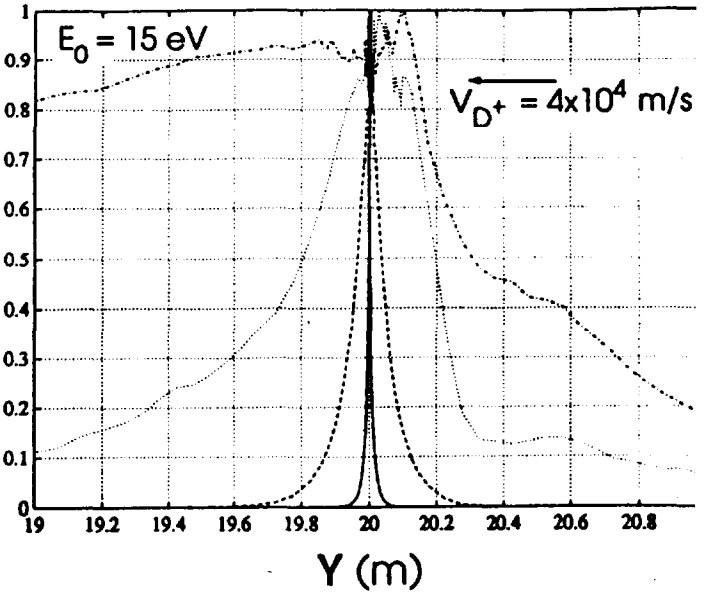
E_0 = 15 eV
V_{D^+} = 4x10^4 m/s
Y (m)

Fig 10

APPENDIX 1.

THE JET TEAM

JET Joint Undertaking, Abingdon, Oxon, OX14 3EA, U.K.

J.M.Adams[1], F.Alladio[4], H.Altmann, R.J.Anderson, G.Appruzzese, W.Bailey, B.Balet, D.V.Bartlett, L.R.Baylor[24], K.Behringer, A.C.Bell, P.Bertoldi, E.Bertolini, V.Bhatnagar, R.J.Bickerton, A.Boileau[3], T.Bonicelli, S.J.Booth, G.Bosia, M.Botman, D.Boyd[31], H.Brelen, H.Brinkschulte, M.Brusati, T.Budd, M.Bures, T.Businaro[4], H.Buttgereit, D.Cacaut, C.Caldwell-Nichols, D.J.Campbell, P.Card, J.Carwardine, G.Celentano, P.Chabert[27], C.D.Challis, A.Cheetham, J.Christiansen, C.Christodoulopoulos, P.Chuilon, R.Claesen, S.Clement[30], J.P.Coad, P.Colestock[6], S.Conroy[13], M.Cooke, S.Cooper, J.G.Cordey, W.Core, S.Corti, A.E.Costley, G.Cottrell, M.Cox[7], P.Cripwell[13], F.Crisanti[4], D.Cross, H.de Blank[16], J.de Haas[16], L.de Kock, E.Deksnis, G.B.Denne, G.Deschamps, G.Devillars, K.J.Dietz, J.Dobbing, S.E.Dorling, P.G.Doyle, D.F.Düchs, H.Duquenoy, A.Edwards, J.Ehrenberg[14], T.Elevant[12], W.Engelhardt, S.K.Erents[7], L.G.Eriksonn[5], M.Evrard[2], H.Falter, D.Flory, M.Forrest[7], C.Froger, K.Fullard, M.Gadeberg[11], A.Galetsas, R.Galvao[8], A.Gibson, R.D.Gill, A.Gondhalekar, C.Gordon, G.Gorini, C.Gormezano, N.A.Gottardi, C.Gowers, B.J.Green, F.S.Griph, M.Gryzinski[26], R.Haange, G.Hammett[6], W.Han[9], C.J.Hancock, P.J.Harbour, N.C.Hawkes[7], P.Haynes[7], T.Hellsten, J.L.Hemmerich, R.Hemsworth, R.F.Herzog, K.Hirsch[14], J.Hoekzema, W.A.Houlberg[24], J.How, M.Huart, A.Hubbard, T.P.Hughes[32], M.Hugon, M.Huguet, J.Jacquinot, O.N.Jarvis, T.C.Jernigan[24], E.Joffrin, E.M.Jones, L.P.D.F.Jones, T.T.C.Jones, J.Källne, A.Kaye, B.E.Keen, M.Keilhacker, G.J.Kelly, A.Khare[15], S.Knowlton, A.Konstantellos, M.Kovanen[21], P.Kupschus, P.Lallia, J.R.Last, L.Lauro-Taroni, M.Laux[33], K.Lawson[7], E.Lazzaro, M.Lennholm, X.Litaudon, P.Lomas, M.Lorentz-Gottardi[2], C.Lowry, G.Magyar, D.Maisonnier, M.Malacarne, V.Marchese, P.Massmann, L.McCarthy[28], G.McCracken[7], P.Mendonca, P.Meriguet, P.Micozzi[4], S.F.Mills, P.Millward, S.L.Milora[24], A.Moissonnier, P.L.Mondino, D.Moreau[17], P.Morgan, H.Morsi[14], G.Murphy, M.F.Nave, M.Newman, L.Nickesson, P.Nielsen, P.Noll, W.Obert, D.O'Brien, J.O'Rourke, M.G.Pacco-Düchs, M.Pain, S.Papastergiou, D.Pasini[20], M.Paume[27], N.Peacock[7], D.Pearson[13], F.Pegoraro, M.Pick, S.Pitcher[7], J.Plancoulaine, J-P.Poffé, F.Porcelli, R.Prentice, T.Raimondi, J.Ramette[17], J.M.Rax[27], C.Raymond, P-H.Rebut, J.Removille, F.Rimini, D.Robinson[7], A.Rolfe, R.T.Ross, L.Rossi, G.Rupprecht[14], R.Rushton, P.Rutter, H.C.Sack, G.Sadler, N.Salmon[13], H.Salzmann[14], A.Santagiustina, D.Schissel[25], P.H.Schild, M.Schmid, G.Schmidt[6], R.L.Shaw, A.Sibley, R.Simonini, J.Sips[16], P.Smeulders, J.Snipes, S.Sommers, L.Sonnerup, K.Sonnenberg, M.Stamp, P.Stangeby[19], D.Start, C.A.Steed, D.Stork, P.E.Stott, T.E.Stringer, D.Stubberfield, T.Sugie[18], D.Summers, H.Summers[20], J.Taboda-Duarte[22], J.Tagle[30], H.Tamnen, A.Tanga, A.Taroni, C.Tebaldi[23], A.Tesini, P.R.Thomas, E.Thompson, K.Thomsen[11], P.Trevalion, M.Tschudin, B.Tubbing, K.Uchino[29], E.Usselmann, H.van der Beken, M.von Hellermann, T.Wade, C.Walker, B.A.Wallander, M.Walravens, K.Walter, D.Ward, M.L.Watkins, J.Wesson, D.H.Wheeler, J.Wilks, U.Willen[12], D.Wilson, T.Winkel, C.Woodward, M.Wykes, I.D.Young, L.Zannelli, M.Zarnstorff[6], D.Zasche[14], J.W.Zwart.

PERMANENT ADDRESS

1. UKAEA, Harwell, Oxon. UK.
2. EUR-EB Association, LPP-ERM/KMS, B-1040 Brussels, Belgium.
3. Institute National des Récherches Scientifique, Quebec, Canada.
4. ENEA-CENTRO Di Frascati, I-00044 Frascati, Roma, Italy.
5. Chalmers University of Technology, Göteborg, Sweden.
6. Princeton Plasma Physics Laboratory, New Jersey, USA.
7. UKAEA Culham Laboratory, Abingdon, Oxon. UK.
8. Plasma Physics Laboratory, Space Research Institute, Sao José dos Campos, Brazil.
9. Institute of Mathematics, University of Oxford, UK.
10. CRPP/EPFL, 21 Avenue des Bains, CH-1007 Lausanne, Switzerland.
11. Risø National Laboratory, DK-4000 Roskilde, Denmark.
12. Swedish Energy Research Commission, S-10072 Stockholm, Sweden.
13. Imperial College of Science and Technology, University of London, UK.
14. Max Planck Institut für Plasmaphysik, D-8046 Garching bei München, FRG.
15. Institute for Plasma Research, Gandhinagar Bhat Gujat, India.
16. FOM Instituut voor Plasmafysica, 3430 Be Nieuwegein, The Netherlands.
17. Commissiariat à L'Energie Atomique, F-92260 Fontenay-aux-Roses, France.
18. JAERI, Tokai Research Establishment, Tokai-Mura, Naka-Gun, Japan.
19. Institute for Aerospace Studies, University of Toronto, Downsview, Ontario, Canada.
20. University of Strathclyde, Glasgow, G4 ONG, U.K.
21. Nuclear Engineering Laboratory, Lapeenranta University, Finland.
22. JNICT, Lisboa, Portugal.
23. Department of Mathematics, Univeristy of Bologna, Italy.
24. Oak Ridge National Laboratory, Oak Ridge, Tenn., USA.
25. G.A. Technologies, San Diego, California, USA.
26. Institute for Nuclear Studies, Swierk, Poland.
27. Commissiariat à l'Energie Atomique, Cadarache, France.
28. School of Physical Sciences, Flinders University of South Australia, South Australia SO42.
29. Kyushi University, Kasagu Fukuoka, Japan.
30. Centro de Investigaciones Energeticas Medioambientales y Techalogicas, Spain.
31. University of Maryland, College Park, Maryland, USA.
32. University of Essex, Colchester, UK.
33. Akademie de Wissenschaften, Berlin, DDR.

CR 88.49.1A